

Study and modeling of eutrophication-related changes in coastal planktonic food-webs

A contribution of the AMORE (Advanced MOdeling and Research on Eutrophication) consortium

SUSTAINABLE MANAGEMENT OF THE NORTH SEA

BELGIAN SCIENCE POLICY

SCIENTIFIC SUPPORT PLAN FOR A SUSTAINABLE DEVELOPMENT POLICY (SPSD-I)

Programme: “Sustainable management of the North Sea”

Study and modeling of eutrophication-related changes in coastal planktonic food-webs

A contribution of the AMORE (Advanced MOdeling and Research on Eutrophication) consortium

*Christiane Lancelot¹, Véronique Rousseau¹, Sylvie Becquevort¹, Jean-Yves Parent¹, Gaele Déliat¹, Caroline Leblanc¹
Marie-Hermande Daro², Stéphane Gasparini², Elvire Antajan², Alan Meyer²,
Kevin Ruddick³, José Ozer³
Yvette Spitz⁴*

¹Université Libre de Bruxelles, Ecologie des Systèmes Aquatiques, CP-221, bd du Triomphe, B-1050, Belgium

² Vrij Universiteit Brussel, laboratorium Voor Ekologie And Systematiek,, Pleinlaan, 2, B-1050, Belgium

³Belgian Royal Institut of Natural Science, Management Unit of North Sea Mathematical Models, Gulledele 100, B-1200

⁴Oregon State University, College of Oceanic and Atmospheric Sciences, USA

1	ABSTRACT	2
2	INTRODUCTION	5
3	MATERIAL AND METHODS	7
3.1	Field sampling	7
3.2	Analytical methods	8
3.2.1	Physico-chemical parameters	8
3.2.2	Biomass of the tropho-dynamic groups	9
3.3	Biological activities	11
3.3.1	Primary production.....	11
3.3.2	Bacterioplankton production.....	12
3.3.3	Copepod grazing and egg production	12
3.3.4	Nano-and micro- grazing	14
3.3.5	Particle potential sinking rates	14
3.4	Mathematical modeling	14
3.4.1	The 3D-COHSNS hydrodynamic model	14
3.4.2	The ecological MIRO model.....	16
3.4.2.1	The basic model and the implementation procedure	16
3.4.2.2	Parameter optimisation and errors estimation	17
3.4.3	The 3D-MIRO&CO model	20
4	RESULTS AND DISCUSSION	21
4.1	Improved knowledge of the eutrophication process in the Belgian coastal waters	21
4.1.1	Nutrient enrichment status of BCZ	21
4.1.2	Response of phytoplankton blooms to nutrient enrichment	23
4.1.2.1	Diatom- <i>Phaeocystis</i> colony successions	23
4.1.2.2	Control of diatom and <i>Phaeocystis</i> colony blooms	24
4.1.3	Fate of ungrazed <i>Phaeocystis</i> -derived organic matter.....	31
4.1.3.1	Spring C budget and trophic efficiency of the planktonic food web	31
4.1.3.2	Origin and biodegradability of dissolved organic carbon in BCZ during the wax and wane of <i>Phaeocystis</i> bloom	34
4.1.3.3	Potential sinking rate of phytoplankton-derived particles.....	36
4.2	Modelling <i>Phaeocystis</i> blooms in BCZ	38
4.2.1	Upgrading and performance of the ecological model 0D-MIRO	38
4.2.1.1	Model structure and parameterisation	38
4.2.1.2	Model implementation.....	43
4.2.1.3	Model results	43
4.2.1.4	Data assimilation: identification of important ecological parameters and errors estimation	47
4.2.2	Development and performance of the 3D MIRO&CO model	52
4.2.2.1	3D-COHSNS hydrodynamical modelling.....	52
4.2.2.2	3D MIRO&CO ecological modelling	55
4.2.3	Nutrient reduction scenarios	58
5	CONCLUSION	60
5.1	Eutrophication status of Belgian coastal waters	60
5.1.1	Nutrient enrichment and algal blooms	60
5.1.2	Increased understanding of bottom-up controls of diatom/ <i>Phaeocystis</i> colony successions	60
5.1.3	Food-web structure and trophic efficiency	61
5.2	Assessment and mitigation tools	63
5.2.1	Prediction capability	63
5.2.2	Mitigation	64
6	ACKNOWLEDGEMENT	64
7	REFERENCES	64

1 ABSTRACT

AMORE (Advanced Modeling and Research on Eutrophication) is an interdisciplinary consortium composed of biologists and physical and ecological modellers focusing their research activities on coastal eutrophication in the Belgian coastal zone (BCZ) with special interest in harmful *Phaeocystis* colony blooms. The long-term objective of AMORE is to develop a mathematical model able to predict the magnitude and geographical extent of *Phaeocystis* colony blooms in the Eastern Channel and Southern Bight of the North Sea with focus on the BCZ in response to varying short-term climate conditions and riverine nutrient (N, P, Si) loads. To achieve this objective AMORE has developed an integrated research methodology that involves and combines in an interactive way the collection of historical and new field data, process-level studies, mathematical modelling and data assimilation.

Between 1997 and 2001 AMORE research focused on mechanisms through which a change in riverine nutrient loads induces modification in the phytoplankton community structure and how this change affects in turn the structure and functioning of the planktonic food-web and the related biogeochemical cycles. The knowledge gained was synthesized for integration in the existing ecological MIRO which in turn was coupled with the 3D-COHSNS hydrodynamical model developed for describing water transport in the studied domain. Progress achieved in our understanding of eutrophication mechanisms in the BCZ as well as our present ability to predict *Phaeocystis* spreading and magnitude in response to riverine nutrient delivery are discussed in the present report.

Among bottom up factors (light, temperature, nutrients) that currently control phytoplankton blooms we demonstrated that a light threshold of $12 \mu\text{mole m}^{-2} \text{s}^{-1}$ in the water column is critical for the onset of the spring phytoplankton bloom in BCZ. This threshold is reached between mid-February and mid-March and relies on physical processes determining the load of suspended matter. This light level corresponds to the light required by early spring diatoms for an optimised cell division rate. These early spring diatoms are also better competitive compared to *Phaeocystis* colonies at the low temperature of late-February early March (5-6°C). On the contrary, *Phaeocystis* colonies optimise their growth at higher temperature and light but are better flexible to light change due to a fast xanthophyll cycling rate. Nutrients availability on the other hand is driving the succession of diatom species and *Phaeocystis*. Diatom blooms are characterized by the succession of three different communities characterized by a specific Si stoichiometry. The observed relationship between the silicification level of diatom species and ambient silicic acid strongly suggests that this nutrient is shaping the observed spring-to-summer diatom

succession in BCZ. Further observational evidence showed that the magnitude of the early spring diatoms is controlled by the availability of Si(OH)_4 and PO_4 to a less extent. This observation, also supported by 0D-MIRO model runs, suggests that “excess new nitrates” (i.e. left over after early spring diatom growth) but regenerated PO_4 and Si (for diatoms only) sustain the growth of *Phaeocystis* colonies and the co-occurrent diatoms (*Guinardia sp.*). For the first time, PO_4 limitation was demonstrated in the BCZ *via* the detection of alkaline phosphatase activity in spring. One major result is that this enzymatic activity is associated to mainly large particles including phytoplankton cells and their attached bacteria. The highly significant correlation between alkaline phosphatase activity and *Phaeocystis* suggests that the colonies might play a major role in PO_4 regeneration.

Specific grazing experiments conducted during AMORE clearly demonstrated that *Phaeocystis* colonies are not grazed by indigenous zooplankton (*Temora longicornis*) but the reason was not identified. The combination of all biological activities and biomass measured in 1998 allowed calculating the budget of carbon transfer through the planktonic network. This calculation indicated that most of ungrazed *Phaeocystis* flows through the microbial network where *Phaeocystis* cells are grazed by microzooplankton and *Phaeocystis*-derived organic carbon is rapidly recycled. This conclusion was supported by independent microbiological assays which suggested that most of organic matter synthesised during the spring bloom was biodegradable *per se*. The very low bacterial growth yield of 0.1 indicates that most organic carbon taken up is mineralised rather than building biomass. This could be due to PO_4 limitation although not experimentally demonstrated. Also in agreement with conclusions of carbon budget calculation, are the negative potential sinking rates obtained for *Phaeocystis* colonies larger than 250 μm . Based upon this carbon budget, it was further hypothesized that adult copepods would be in food shortage during *Phaeocystis* blooms which could impact negatively not only on the next generation of copepods but also on fish recruitment by starvation of fish larvae. This hypothesis was however challenged by additional field data on egg production by copepods suggesting alternate sources of good quality food for copepods. Yet the trophic pathways are even more complex due to the presence between April and June of an impressive mass of gelatinous zooplankton which trophic role was not identified.

Numerical experiments included 0D and 3D modelling. Prior to its 3D implementation, the published version of 0D-MIRO was upgraded based on a synthesis of process-level studies and making use of data assimilation technics. For this purpose the adjoint model of 0D-MIRO was set up and twin experiments were conducted to improve MIRO parameters and estimate possible error due to some unresolved physical processes in 0D. From this numerical work the independence of all MIRO

parameters was demonstrated and the most important parameters of the ecosystem functioning were highlighted. 3D-MIRO&CO was implemented by coupling the upgraded version of MIRO to the 3D-COHSNS hydrodynamical model. The modelled domain was bordered by latitudes 51°N and 52.5°N and included input from the main rivers within this domain (Rhine, Scheldt, Thames). For this first application the grid resolution was 4.5km. Simulations were run for the years 1995-1998 and sensitivity studies conducted to assess the relative importance of wind, tide, and river discharge on physical features and nutrient discharge on ecosystem dynamics. Main results obtained show that the geographical extent of the plume of continental coastal freshwater in BCZ depends mainly on wind speed and direction, and is only weakly dependent on tide and river flow-rate (which affects absolute salinity but not dispersion of freshwater). In contrast to currently admitted opinion, freshwater found in the central BCZ at station 330 originates primarily from the Rhine discharge and salinity at station 330 is only slightly affected by discharge from the river Scheldt. However and contrarily to the salinity fields, plumes of nutrients from the rivers Scheldt and Rhine remain relatively distinct (not merged) because of winter depletion. Impact of Scheldt nutrient discharge on BCZ remains important, though the Rhine discharge needs also to be considered. Simulations of biological variables with 3D-MIRO&CO demonstrated a number of observed processes such as the diatom-*Phaeocystis* succession and the related depletion of silicates and nitrates and gave for the first time a view of spatial variability within the domain. However, a number of model weaknesses were also identified which require in part a better understanding and parameterisation of biological processes. These are for instance the parameterization of mesozooplankton feeding and of processes involved in phosphorus benthic diagenesis.

Finally model results obtained with NO₃ and/or PO₄ reduction scenarios suggest that NO₃ discharged by the Scheldt river should be the target nutrient to be reduced for obtaining a significant decrease of *Phaeocystis* colony blooms in the BCZ.

NO₃ discharged by the Scheldt river should be the target nutrient to be reduced for obtaining a significant decrease of *Phaeocystis* colony blooms in the BCZ.

2 INTRODUCTION

The coastal zone, at the interface between land, ocean and atmosphere, plays a major role as recipient of large amounts of nutrients from human activities, including industrial effluents, agricultural runoff, and municipal sewage. Manifest effects of man-induced coastal eutrophication usually appear as qualitative changes of pelagic food-webs with resulting undesirable effects (e.g. proliferations of undesirable or toxic phytoplankton species, extinctions of key species at higher trophic levels, reduced yields of harvestable fish or invertebrate populations...). This alteration of the ecosystem structure and function is primarily driven by changes in nutrient ratios available to coastal phytoplankton over-enriched in nitrogen and phosphorus and deficient in silicon compared to diatom needs (Brzezinski, 1985). Anthropogenic inputs thus stimulate the development of opportunistic large non-siliceous phytoplankton, with high resistance to direct grazing pressure and fast biodegradation (e.g. Lancelot, 1995). Man-induced coastal eutrophication is then accompanied by major changes in the flows of energy and materials within the system, affecting the global significance of coastal seas in terms of natural resources (water quality and harvestable biological resources), nutrient retention, and carbon exportation/sequestration and of greenhouse gases emitters.

The Belgian Coastal Zone (BCZ) is one example of nutrient-enriched coastal sea invaded every spring by massive algal blooms reaching biomass higher than 30 mg Chl a m⁻³. The BCZ, located in the eastern Southern Bight of the North Sea, is a highly dynamic system with waters resulting from the mixing between the in-flowing Atlantic waters and freshwater river inputs (Fig.1). Overall the nutrient enrichment in the BCZ reflects the cumulative inputs from atmospheric and riverine sources, local benthic remineralization and the in-flowing Atlantic waters themselves enriched by nutrient loads primarily from the river Seine mainly. The relative importance of these different sources in the BCZ is not accurately known. However atmospheric loads are negligible when compared to transboundary and Scheldt inflows (less than 1%; Rousseau et al., 2003). Eutrophication along the continental coastline of the Southern Bight of the North Sea manifests as huge algal spring blooms (mainly the Haptophyceae *Phaeocystis globosa*) that spread over the whole area along a SW-NE gradient (Lancelot et al., 1987). Current knowledge reports that the massive development of *Phaeocystis* colonies after the early spring bloom of diatoms is sustained by freshwater sources of nutrients, deficient in silicon compared to nitrogen and phosphorus (Lancelot et al., 1997). To what extent this change in phytoplankton community structure affects ecosystem structure and function and hence the overall yield of harvestable biological resources is not known yet. Observational evidence of complex changing planktonic food-webs does however exist (Hansen et al., 1992;

Rousseau et al., 2000). Due to the complexity of bottom-up and top-down controls of marine planktonic food webs, the link between nutrient change and the coastal ecosystem function cannot be understood by simple correlation between events. Mechanistic models which are based on chemical and biological principles and describe ecosystem carbon and nutrient cycles as a function of environmental pressure are ideal tools to handle this complexity. These models are evolving conceptual tools integrating the current knowledge of ecosystem functioning. For this reason they are powerful tools for basic research identifying new research requirements by comparison between model results and observations and by model sensitivity studies. When validated these models can be used to better understand the dynamics of the ecosystem and assess the magnitude and extent of harmful algal blooms and the related impact in response to changes in land-based nutrients and climate.

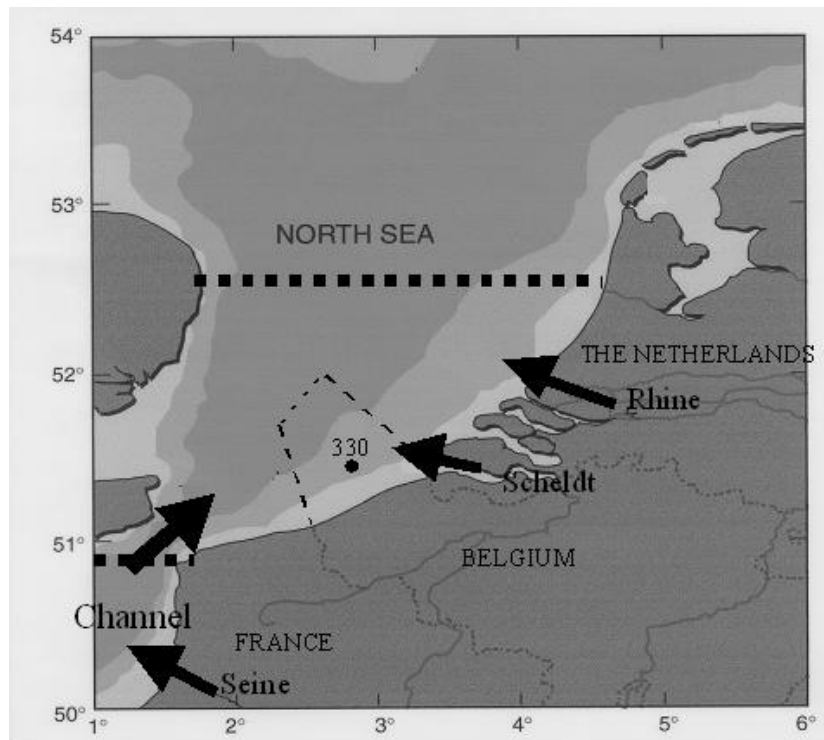


Figure 1: Map showing the Southern Bight of the North Sea (horizontal dotted lines show the limit of the modelled domain), the Belgian coastal zone (dotted contour) with location of station 330. Arrows indicate the SW Atlantic inflow and discharge of main rivers.

Constructing a mechanistic model, the MIRO model, able to describe *Phaeocystis* blooms in the nutrient-enriched BCZ is the purpose of AMORE (Advanced Modeling and Research on Eutrophication), an interdisciplinary consortium composed of biologists and physical and ecological modelers and focusing their research activities on coastal eutrophication with special interest in harmful algal blooms. To achieve this long term objective AMORE implemented an integrated research methodology that includes and combines field observation, process-level studies and ecological modeling. On the long term however progress achieved by AMORE will help assessing (i) the natural capacity of coastal ecosystems to assimilate nutrients originating from land-based sources; (ii) the level of nutrient reduction required to protect living resources from the harmful effects of nutrient enrichment; (iii) the assessment and monitoring of positive/negative effects of current nutrient reduction programs, all needed to secure sustainable development of marine resources in the region.

Between 1997 and 2001 AMORE investigations especially focused on mechanisms through which a change in nutrient loads induces modification in the phytoplankton community structure and how this change affects in turn the structure and functioning of the planktonic food-web and the related biogeochemical cycles. Progress achieved is discussed in the present report in terms of nutrient enrichment and algal blooms, food-web structure and trophic efficiency and prediction capability of mathematical models.

3 MATERIAL AND METHODS

3.1 Field sampling

Field work was conducted aboard RV Belgica and Zeeleeuw. Due to the complex dynamic of the BCZ, the chosen sampling strategy included a high-time resolution survey of surface water core physico-chemical and biological parameters at a reference station for BCZ and seasonal measurements of targeted biological activities along inshore-offshore gradients (geographical sampling). Sampling was limited to surface waters as the strong alongshore tidal currents (1 m s^{-1}) combined to the shallow water depths ensure a permanent vertical mixing of the water column (Creutzberg & Postma, 1979).

The time series monitoring was conducted at station 330 (N $51^{\circ}26.05$; E $002^{\circ} 48.50$; Fig. 2). This station occupies a central position in BCZ and has been sampled

regularly since 1989. Between 1993 and 2000, station 330 was sampled weekly to biweekly. Surface seawater was collected with a bucket in order to avoid disruption of colonies and analysed for major nutrients, suspended matter, temperature, salinity, Chl. a and phytoplankton.

The geographical field campaigns took place in spring and summer (from March to July) between 1998 and 2001. In 2001 winter and fall sampling was conducted as well for measuring zooplankton winter activity. The geographical grid (Fig. 2) was chosen along inshore-offshore gradients in order to sample water of different influences (Atlantic vs Scheldt and Rhine). During these cruises different instruments (Niskin bottles at different depths, plankton nets, snow catcher) were deployed for collecting the different biological organisms under study.

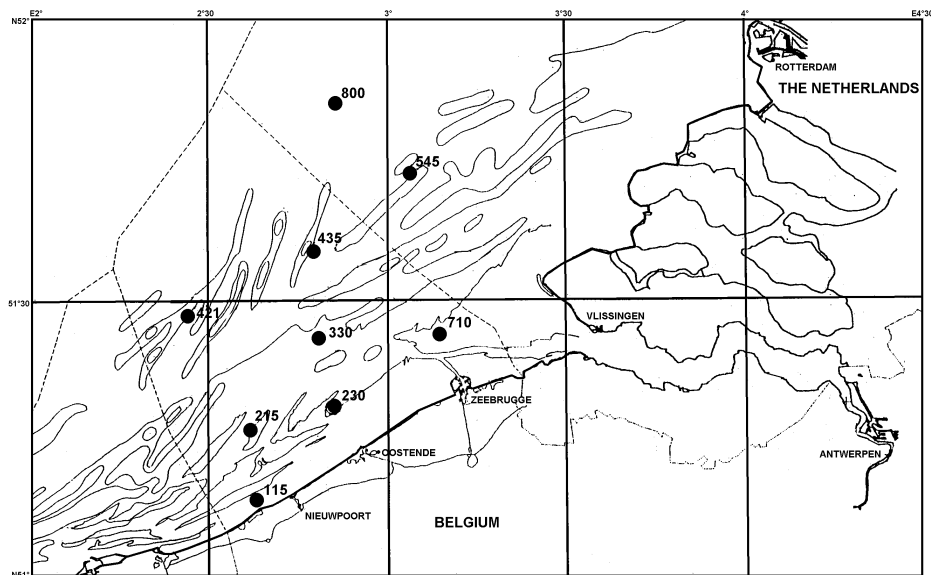


Figure 2: map of the Belgian coastal zone with location of sampling stations. The dashed line shows the limits of the Belgian Economical Exclusive Zone

3.2 Analytical methods

3.2.1 Physico-chemical parameters

Seawater temperature and salinity were measured aboard with a thermosalinometer (Beckman). Major nutrient [NO_3 , NH_4 , $\text{Si}(\text{OH})_4$ and PO_4] concentrations were determined on 0.45 μm filtered seawater according to the colorimetric methods described in Grasshof et al. (1983). Additionally, for days when biological processes

were investigated, irradiance was continuously measured using a cosine sensor (LiCor).

Pigments were determined on 90 % (v:v) acetone extracted particulate material isolated by filtration on glass fiber filters (GF/C, Whatman). Chlorophyll a (Chl a) concentration was routinely determined by spectrometry using the method and equations recommended by Lorenzen (1967). Pigments concentration was measured by High Performance Liquid Chromatography (HPLC) using the Spherisorb ODS2 reverse-phased column and the solvent system of Wright et al., 1991).

Biogenic silica (BSi) was determined on particulate material collected on 47 mm diameter polycarbonate membrane filters (0.6 μm pore size; Nuclepore). Filters were dried immediately at 50°C for 12h, and stored at room temperature in sealed Petri dishes until analysis. BSi concentrations were determined according to the sequential Na(OH)/HF digestion method (Ragueneau and Tréguer, 1994). This method allows the determination of a factor correcting the particulate silica extracted during the NaOH digestion for the leaching of lithogenic Si (LSi). In accordance, that the contribution of LSi to BSi in the central BCZ (station 330) was estimated at 28% (Rousseau et al., 2002).

Dissolved organic carbon (DOC) was determined on pre-ashed GF/F filtered seawater using the high-temperature catalytic oxidation (HTCO) technique (Sugimura & Suzuki, 1988; Suzuki, 1993). Total dissolved carbohydrates (TDCHO) were measured according to the spectrophotometrical method of Myklestad et al. (1997) after a 0.1 N HCl hydrolysis (final concentration, 150°C, 1 h). The biodegradable fraction of DOC was investigated with microbial bioassays adapted from Servais et al. (1987). Field water was sterilized by filtration through a polycarbonate membrane (Nuclepore, 0.2 pore size, 90-mm diameter) previously acid washed (HCl 10 %), and abundantly rinsed with MilliQ water. The filtrate was seeded with native bacterial assemblage (5-10 % v/v) obtained by filtration through a polycarbonate membrane ((Nuclepore, 0.8 pore size, 90-mm diameter). This filtration allows to discarding particulate matter and bacterial grazers (Servais et al., 1989; Block et al., 1992). Bioassays were incubated in the dark at 19°C for a period of 30 days. DOC and total dissolved carbohydrates (TDCHO) were measured at day 0 and 30. DOC30 represents the refractory fraction of the bulk DOC after 30 days and the biodegradable dissolved organic carbon (BDOC30) or biodegradable TDCHO (BTDCHO30) are estimated by difference between measurements at day 0 and 30.

3.2.2 Biomass of the tropho-dynamic groups

Depending on the organisms, specific procedures were used for sampling, preservation, storage and microscopic analysis. Diatoms, *Phaeocystis* colonies and

microprotozooplankton were enumerated under an inverted microscope (Leitz Fluovert) according to Utermöhl method (Hasle, 1978). Samples were preserved with 1 % (final concentration) lugol-glutaraldehyde solution and stored at 4°C in the dark until analysis. Magnification was chosen according to cell or colony size: 40 or 100 X for *Phaeocystis* colonies; 100 or 200 X for diatoms or protozoa and 320 X for cells ranging in the size range 20-50 µm. In total, at least 400 cells were enumerated with 100 cells of the most abundant genus or species. Diatoms were enumerated and identified according to the genus level unless a species was easily identifiable or dominant. Their carbon biomass (C-biomass) was calculated on the basis of cell density and biometric factors determined for each species or genus. A specific average conversion factor was calculated from biovolumes measured on a cell population throughout the period of its development. Biovolumes were then converted using a carbon content factor of 0.11 pgC µm⁻³ of plasma volume (Edler, 1979). *Phaeocystis* was identified as *P. globosa* and will here be referred as *Phaeocystis*. Colony cell number was determined according to the method described in Rousseau et al. (1990). *Phaeocystis* colony C-biomass was estimated from biovolume measurement according to the empirical procedures of Rousseau et al. (1990) and van Rijssel et al. (1997). These two methods reflect different approaches of the colony structure based on the existing knowledge. In 1990, Rousseau et al. considered *Phaeocystis* colonies as jelly spheres with cells embedded in mucus and derived the measurement of cellular and mucilaginous C-biomass from colony biovolume. Later, with the development of confocal laser scanning imagery combined to biochemical analysis, van Rijssel et al. (1997) demonstrated the hollow structure of *Phaeocystis* colonies, also confirmed by Hamm et al. (1999), with cells embedded in a 7 µm membrane-like structure. On this basis, a constant carbon content of 57 pg C cell⁻¹ was experimentally determined for the Southern North Sea colonies (van Rijssel et al., 1997). Analysis of both calculations (not shown) indicates that the two methods are comparable for natural colony assemblages with an average diameter of less than 700 µm. For higher average diameter, the method of Rousseau et al. (1990) estimates 30 % higher C concentrations. Microprotozooplankton C-biomass was calculated by using the conversion factor 0.19 pgC µm⁻³ (Putt & Stoecker, 1989) and 0.13 pgC µm⁻³ (Edler, 1979) for respectively ciliates and dinoflagellates.

Bacteria, auto- and hetero-trophic nanoflagellates were enumerated by epifluorescence microscopy after DAPI staining following the method of Porter & Feig (1980). Samples were preserved with 40 % formaldehyde (final concentration 2 %) and 25 % glutaraldehyde (final concentration 0.5 %) for bacteria and flagellates, respectively. Bacteria were enumerated on 10 different fields at 1000 X magnification. Biovolumes were calculated by treating rods and cocci, respectively,

as cylinders and spheres (Watson et al., 1977) and converted to C-biomass by using the biovolume dependant conversion factor established by Simon & Azam (1989). At least 100 flagellates were counted and autotrophs were discriminated from heterotrophs by the red chlorophyll autofluorescence. C-biomasses were calculated from cell density and biometric factors by using the factor 0.11 pgC μm^{-3} of Edler (1979).

About 50-100 liters of water were filtered through a 50 μm size mesh net for enumeration of copepod nauplii and copepodites I-II stages as well as other small metazooplankton. A 300 μm size mesh net equipped with a flow meter was used to sample larger stages of mesozooplankton. All samples were preserved with formaline (4 % final concentration). Small and large metazooplankton were identified to species level and enumerated under stereoscopic microscope. C-biomass was calculated using species- and stage- specific dry weight measured for the dominant metazooplankton species of the Belgian coastal waters (Daro and van Gijsegem, 1984).

3.3 Biological activities

Daily primary production, bacterial production and meso-zooplankton grazing were experimentally determined under simulated *in situ* conditions.

3.3.1 Primary production

Daily photosynthesis, growth, respiration and exudation rates of phytoplankton were determined from ^{14}C radiotracer experiments using the method described in Mathot et al. (1992) and the AQUAPHY set of equations of Lancelot et al. (1991). The experimental protocol involved two radiotracer experiments run in parallel for each sampled phytoplankton community. Photosynthetic characteristics were determined from short-term (2 h) experiments of ^{14}C uptake at different light intensities (P/E curve). Growth, exudation and respiration were assessed by running 24h-time course experiment of ^{14}C incorporation into phytoplanktonic cellular components (small metabolites, proteins, polysaccharides, lipids) during a natural day light cycle according to the protocol of Lancelot & Mathot (1985). AQUAPHY parameters were determined by mathematical fitting of ^{14}C experimental data using the equations described in Lancelot et al. (1991). Particular attention was given to select samples with a clear dominance of either diatoms or nanophytoplankton or *Phaeocystis* colonies. Daily rates of each community were then calculated by integration on the variations of light in time and within depth of the AQUAPHY set of equations with the relevant parameters, making use of *in situ* biomass, temperature and nutrients.

The method of Tréguer et al. (1991) based on ^{32}Si -silicic acid uptake was occasionally used to estimate specifically the growth rate and Si:C stoichiometry of natural diatom assemblages (Rousseau et al., 2002). Parallel 24h-kinetics experiments of ^{32}Si uptake and ^{14}C incorporation into proteins, as an index of phytoplankton biomass production, into diatom-dominated natural communities were conducted in simulated natural conditions. The ^{32}Si incorporation by diatoms was estimated by detection of the Cerenkov radiation (Packard Tri-Carb 1600CA) of the daughter ^{32}P after secular equilibrium was reached (about 4 months).

3.3.2 Bacterioplankton production

Bacterioplankton production was determined by ^3H -leucine incorporation into proteins and ^3H -thymidine into DNA according to the protocol described in Becquevort et al. (1998). Leucine and thymidine incorporation rates were converted into bacterial production using the following conversion factors established for the North Sea bacterial communities by Servais (1990): 3950 gC produced per mole of leucine incorporated into proteins and 2.66×10^{18} bacteria produced per mole of thymidine incorporated in the cold TCA insoluble material.

In order to investigate the spring phosphate limitation and assess the respective role of bacteria and phytoplankton in organic phosphorus hydrolysis, measurements of alkaline phosphatase activity (APA) were conducted during periods of *Phaeocystis* dominance. APA was measured using fluorescent substrate analogous 4-methylumbelliferyl- Phosphate (MUF-P, Sigma, St. Louis, USA) which produces fluorescent 4-methylumbelliferone after hydrolysis. The procedure was adapted from the protocol of Ammerman (1991). Protocols based on size fractionation were developed to distinguish between free, phytoplankton- and bacterioplankton-surface bound alkaline phosphatase.

3.3.3 Copepod grazing and egg production

Copepod grazing on phyto- and protozooplankton was estimated based on clearance or ingestion rates experimentally determined for each copepod species and stages and the respective prey biomass. Three methods, pigment (HPLC) gut content, ^{14}C -radio-labelled monospecific [*Phaeocystis* small (diameter < 150 μm) and large (> 150 μm), *Chaetoceros socialis*] and mixed [*Thalassiosira fallax* and *T. Nordenskoldii*] prey and cell-count experiments, were used and combined (Gasparini et al., 2000). The ranges of measured clearance rate are reported in Table I and discussed in Gasparini et al. (2000). The daily grazing rate of each species and stage of copepod was then calculated on the basis of the specific biomass, the clearance rates reported in Table I and the prey biomass.

Table I: Range of clearance rates determined by Gasparini et al. (2000) for the different copepod species and stages on the various prey.

Copepod species and stages	Clearance rates, cm ³ ind ⁻¹ h ⁻¹	
	On diatom prey	On microzooplankton prey
<i>Acartia clausi</i>		
III-IV	0.2-0.4	0.2-0.5
V	0.3-0.6	0.3-0.8
Adult	0.6-1.1	0.5-1.4
<i>Temora longicornis</i>		
III-IV	0.4	0.2-0.5
V	0.6	0.2-0.7
Adult	0.8	0.3-1
<i>Centropages hamatus</i>		
III-IV	0.3-0.4	0.6-0.9
V	0.4-0.6	1-1.5
Adult	0.5-0.8	1.2-1.8

The grazing rates of nauplii and copepodite I-II, was estimated based on the clearance rates–prey concentration relationships derived from Daro (1985) :

$$CR_{\text{nauplii}} = 0.135 \cdot 10^{-0.001 p} \quad \text{and} \quad CR_{\text{copepodite I-II}} = 0.442 \cdot 10^{-0.003 p}$$

In which CR_{nauplii} and $CR_{\text{copepodite I-II}}$, expressed in ml ind⁻¹ l⁻¹, are the clearance rates of nauplii and copepodite I-II stages respectively; and p, the prey concentration, in µgC l⁻¹.

Copepod grazing measurements were complemented with egg production experiments to assess food limitation of copepods during *Phaeocystis* bloom. *T. longicornis*, the dominant species in BCZ in Spring was used as model and incubations were run with 5 females in Perspex tubes with 200 µm mesh false bottom to preventing egg cannibalism.

3.3.4 Nano-and micro- grazing

The grazing rates of nano- and micro-protzooplankton were calculated from prey concentrations using relationships describing the dependence of ingestion or clearance rates on prey. These relationships were derived from previous experiments performed on natural populations of prey and grazers in the Belgian coastal waters during the spring bloom period. The Holling type II functional response characterised by a maximum ingestion rate of 64.5 bacteria ingested per nanoprotozooplankton per hour and a half-saturation constant of $7.7 \cdot 10^8$ bacteria l^{-1} (Becquevort, 1987; Lancelot et al., 1991) was used to calculate the nanoprotozooplankton grazing on bacteria. Microprotozooplankton grazing on nanoflagellates was calculated on basis of clearance rates ranging between 3.5 and $15.5 \mu l \text{ ind}^{-1} \text{ h}^{-1}$ for nanophytoplankton concentrations varying from 5 to 62 mgC m^{-3} measured by Weisse & Scheffel-Möser (1990).

3.3.5 Particle potential sinking rates

For the first time in the Belgian coastal waters, the potential sedimentation of phytoplankton and derived aggregates was measured using SETCOL sedimentation columns (SETCOL, Bienfang 1981). In this technique, particles are collected at three depth of the SETCOL (surface, mid, bottom) after 2 hour-sedimentation. Particles are analysed for their content in Chl. a, POC, auto- and hetero-trophic microorganisms.

3.4 Mathematical modeling

A three-dimensional ecological model (3D-MIRO&CO) of high spatial and trophic resolution to resolving the changing nutrients loads, the complex biology and hydrodynamics and the tight coupling between the benthic and pelagic realm that characterizes the BCZ was implemented in AMORE. The model results of the online coupling of the 3D-COHSNS hydrodynamic model and an upgraded version of the ecological model MIRO (Lancelot et al., 1997) based on new knowledge gained from process-level studies and making use of new data assimilation techniques.

3.4.1 The 3D-COHSNS hydrodynamic model

The 3D-COHSNS numerical model (Ruddick et al., 2003) describes the salinity distribution in the Southern Bight of the North Sea (SNS) making use of the 3D-COHERENS hydrodynamic model of Luyten et al (1999). The source code of the standard version of the model is available publicly on CDROM. Basically the 3D

model solves the continuity, momentum and salinity transport equations on a staggered Cartesian, sigma coordinate grid with an explicit mode-splitting treatment of the barotropic and baroclinic modes. Advection of salinity is discretised by a direction-split Total Variation Diminishing (TVD) scheme. Vertical diffusion is modelled using an evolution equation for turbulent kinetic energy and a quasi-parabolic vertical profile for turbulence macrolength scale. Minimal vertical diffusion and viscosity coefficients of $10^{-6}\text{m}^2\text{s}^{-1}$ were used. Horizontal diffusion is not applied explicitly, but the process of horizontal diffusion arising from the combination of horizontal advection with vertical diffusion is resolved. Advection of momentum was treated with a first order upwind scheme. Full details of all these methods as well as the original references can be found in (Ruddick 1995) and (Luyten et al 1999).

In the present application the model has been set up for the region between 51°N and 52.5°N using a horizontal grid with resolution $2.5'$ longitude (approx. 2.8 km) by $1.25'$ latitude (approx. 2.3km) and with 10 vertical sigma coordinate layers. The model is run with mode-splitting time steps of 45s and 450s respectively for 2D and 3D calculations. Results obtained from an operational 2D storm surge model of the North Sea continental shelf (de Vries et al 1995) forced by 6-hourly wind stress and atmospheric pressure fields (UK Meteorological Office) were used as Southern and Northern open sea cross-boundary transport (vertically-integrated current). Temporal interpolation of monthly measurements of flow-rate for the Rhine and Scheldt and a typical annual cycle for the Thames rivers were used to describe the riverine transport. At the two open sea boundaries the vertical current structure is determined by imposing the condition (Deleersnijder et al 1989) of zero normal derivative of the deviation of current from the vertically-averaged horizontal current, while at river boundaries a condition of zero vertical gradient of current is applied. For salinity, zero flux is assumed at the sea bottom and sea surface boundaries. To ensure salt conservation the incoming salinity at the river boundaries is set to zero. At the other open sea boundaries, no boundary condition is required when the current is directed out of the domain. For inflow periods, the salinity at the Southern, « Channel », boundary is specified as 35. At the Northern, « Central North Sea », boundary a salinity of 34.45 is specified West of 4°E , while East of this longitude a zero horizontal gradient of salinity is specified to allow realistic formation of the Rhine plume and associated Dutch coastal current. Initial conditions were obtained by running the 3D-COHSNS model for the period January 1991-December 1992 with open boundary and forcing from the 2D model as described above. A number of simulations were then carried out for the period January-December 1993 with variations in either boundary conditions or model parameters in order to establish the sensitivity of modelled salinity fields and time series.

3.4.2 The ecological MIRO model

3.4.2.1 The basic model and the implementation procedure

The ecological model is an upgraded version of MIRO (Lancelot et al., 1997) and describes and predicts C, N, P and Si cycling through aggregated components of the coastal ecosystem, over seasons and years, in response to the physical and nutrient forcing. This complex model results of the integration of 4 modules describing the dynamics of phytoplankton (3 taxa), zooplankton (2 taxa), dissolved and particulate organic matter degradation and nutrient (NO_3 , NH_4 , SiO, PO_4) regeneration in the water column and the sediment. The MIRO model structure and parameterisations are based on ecological and physiological principles. The model thus synthesises current knowledge on the kinetics and the factors controlling the main auto- and heterotrophic processes involved in the structure and functioning of the *Phaeocystis*-dominated coastal ecosystem. It is continuously in development relying on analysis of model results and progress gained in experimental aquatic ecology especially those obtained by experimental process-level studies described in the present report.

The MIRO model was first calibrated in a 0D frame. For the application of the 0D-MIRO model to the continental coastal waters of the North Sea, a multi-box frame has been considered based the hydrological regime. This simple resolution of the hydrodynamics represents a first approach to this tidally well-mixed area. In order to take into account the cumulated nutrient enrichment of Atlantic waters by the Seine and Scheldt rivers, two successive boxes (FCZ, BCZ), assumed to be homogeneous, have been chosen from the Baie de Seine to the Belgian coastal zone (Fig. 1). The offshore limit of the boxes is taken along a residual streamline so that inshore-offshore exchanges by residual advection can be neglected. Each successive box has its own characteristics (Table II) and is treated as an open system, receiving waters from the Southern adjacent box and exporting water to the Northern one. The seasonal variation of the state variables is calculated by solving the equations expressing mass conservation in the system with an Eulerian time discretisation. Climatological functions calculated from the period 1989-1999 are used for meteorological and river input forcing. These functions were parameterised from recorded daily solar global radiation (meteorological station Oostende, IRM) and seawater temperature, and monthly nutrient loads for the rivers Seine (Cellule Antipollution de Rouen du Service de la navigation de la Seine in France) and Scheldt [Institute for Inland Water Management and Waste Water Treatment (RIZA, The Netherlands) and Department of Environment and Infrastructure (Ministry of Flemish Community, Belgium)]. The latter are directly mixed at each time step (15 minutes) in the relevant boxes. The South-Western (SW) boundary conditions are provided by the results of MIRO calculations performed for the conditions existing in

the western Channel area (WCH), considered as a quasi oceanic closed system. For this application model runs are performed for meteorological conditions of 1989 until a steady state is reached. This occurs after 3 years.

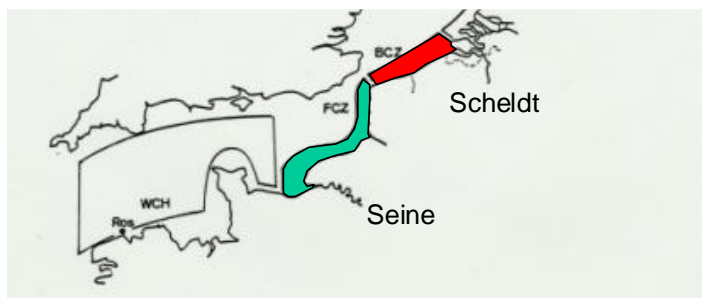


Figure 3: The multi-box implementation domain of MIRO

3.4.2.2 Parameter optimisation and errors estimation

Some of the parameters needed to run the MIRO model are little-known (e.g. sinking rates) or even impossible to measure directly (e.g. mortality rates). In addition, the number of parameters (and their values) needed to describe a biological pathway is dictated by the chosen, often empirical, mathematical formulation. In recent years, data assimilative ecosystem models with parameter estimation have been successfully applied to various regions of the ocean. In addition, several studies used data assimilation as a tool to estimate not only the parameters of the model but also to identify the major pathways of the ecosystem (Hurtt and Armstrong, 1999; Spitz et al. 2001). As a complement to targeted process-level studies we have used the variational adjoint method and nutrients and biological data from one station in the North Sea (Station 330) to estimate the model parameters and identify model pathways that are controlling the behaviour of the ecosystem as well as eventual missing pathways and errors due to missing physical processes (advection/diffusion) in 0D-MIRO.

Basically the variational adjoint method determines an optimal solution by minimizing an objective function, the cost function, which measures the difference between the model solution and the available observations. Two advantages of this technique are its potential application to both linear and non-linear models, and implementation in a straightforward manner. Most minimization algorithms require the computation of the gradient of the cost function with respect to the control variables, e.g. model parameters. The data assimilative model then consists of three components: the forward ecosystem model, the backward model or adjoint model, and an optimisation

procedure (Fig. 4). The three components of the assimilative model are used in an iterative procedure, which leads to the determination of the control variables (e.g. model parameters) giving the best fit to the data and can be described as follows. The direct model is run with an initial guess of the control variables. The model output and data are then used to compute the value of the cost function. Thereafter, the adjoint of the model, run backward in time, gives the gradient of the cost function with respect to the control variables, which is then used in the optimisation procedure to compute the search direction towards the minimum and the optimal step size in that direction. New values of the control variables are then estimated, and the model is re-run. This procedure is applied until a preset convergence criterion is satisfied. In practice, to assure that the cost function has reached a global minimum and not a local minimum, the procedure is repeated with different first guesses of the control variables. The global minimum is reached if all the runs converge towards the same value of the cost function.

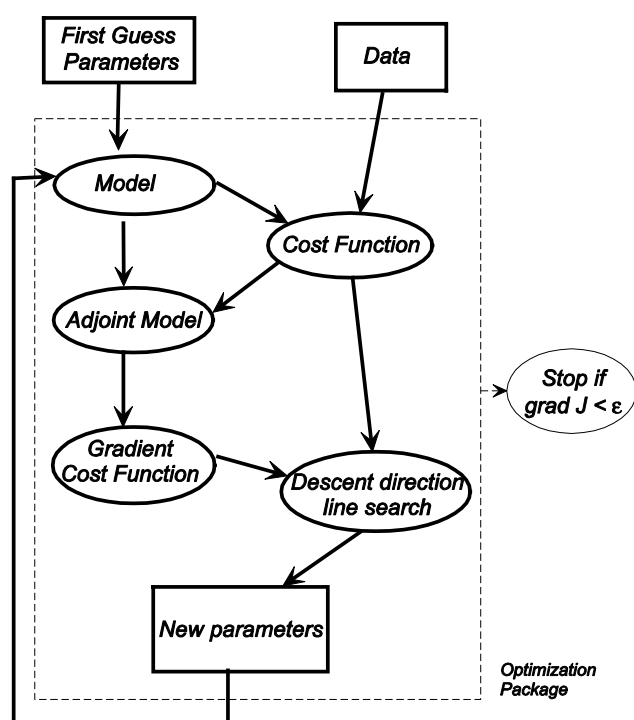


Figure 4: Schematic of the assimilative model. Grad J represents the gradient of the cost function with respect to the model parameters and ϵ is a small value

While the adjoint method is a powerful tool for obtaining the gradient of the cost function with respect to the parameters of the model, the most difficult aspect of this technique is the development of the adjoint model code that is consistent with the direct model code. In this study, the adjoint FORTRAN model code is directly from

the FORTRAN model code based upon the use of Lagrange multipliers Lawson et al. (1995, 1996). This technique provides a straightforward way of writing code and avoids the inconsistency that can occur from the discretisation of the adjoint continuous equations. The optimization procedure uses the subroutine N1QN3 from Gilbert and Lemaréchal (1989), which is based upon a limited memory quasi-Newton method.

In the variational technique, the cost function J is defined in a least squares manner as

$$J = \frac{1}{2} \sum_{i,n} (d_{i,n} - a_{i,n})^T W_i (d_{i,n} - a_{i,n}),$$

where d and a are the data and model equivalents to the data, respectively, i refers to the data types and n refers to the observation time. The weighting matrices W_i are theoretically the inverse of the observation error covariance matrices. By assuming that errors in the data are uncorrelated and have equal variance, the weight matrices can be rewritten as

$$W_i = w_i \mathbf{I},$$

where w_i is a positive scalar and \mathbf{I} is the identity matrix. In practice, w_i takes into account the relative magnitude of the various data types and the quality of the data sets. In this study, w_i accounts for the differences in the relative magnitude observed in the time-average of each data type and is defined as

$$w_i = \frac{\max(\bar{d}_j)}{\bar{d}_i}$$

where \bar{d}_i is the time-average of the observation i and $\max(\bar{d}_j)$ is the maximum of the time-average of the assimilated observations (Lawson et al., 1996). Since we wanted to keep the maximum degree of freedom on the parameters, no a priori information on the parameters is added to the cost function (Fasham and Evans, 1995; Matear, 1995).

Before assimilation experiments, the correctness of the adjoint MIRO code was verified using the procedure developed by Lawson et al. (1995). Then several twin experiments where the observations are the model outputs were conducted. The twin experiments using model-generated observations can be considered as the best scenario where the data set is guaranteed to be consistent with the model, free of measurement error, and expressed in the same units as the model results. This is a necessary step prior to assimilating real observations to verify that the model

parameters are independent, and the observations (time resolution and kind of observations) are sufficient to determine the model parameters and model errors.

3.4.3 The 3D-MIRO&CO model

The upgraded version of MIRO has been coupled to the developed 3D-COHSNS hydrodynamical model (Ruddick et al., 2003): the 3D-MIRO&CO model. The coupled model calculates the vertical and horizontal transport of the ecosystem and biogeochemical state variables. The geographical domain is bordered by latitude 51°N and 52.5°N and is defined by 50 cells (5' longitude) in the East-West direction, 37 cells (2.5' latitude) in the North-South direction and 5 vertical sigma layers (1/5th of the total water depth each). A time step of 900s is used to ensure numerical stability of the scheme used for advection of scalars, including biological state variables.

The model is constrained with 6-hourly wind and atmospheric pressure data obtained from the UK Meteorological Office; an imposed, spatially uniform climatological temperature (annual cycle) and surface incident PAR reconstructed from respectively existing seawater temperature data for the region and the Global Solar Radiation data for the 1989-1999 period. Available PAR in the water column is calculated based on an empirically-determined parameterisation of the light extinction coefficient as a function of suspended matter. Seasonal (4 per year) fields of the latter are reconstructed at the grid of the modelled domain from SeaWiFS images.

The open boundary water flows and nutrients were obtained from application of the 2D Continental Shelf model of de Vries et al (1995) and making use of the climatological database compiled in the scope of the NOWESP and ERSEM EU-projects (Radach et al., 1995). A zero horizontal gradient was assumed for biological and organic matter state variables. Monthly-averaged freshwater and nutrient Scheldt discharges were calculated for the period 1989-2000 based on data obtained from the Institute for Inland Water Management and Waste Water Treatment (RIZA, The Netherlands) and Department of Environment and Infrastructure (Ministry of Flemish Community, Belgium). Monthly-averaged freshwater and nutrient Rhine and Thames loads were estimated from measured discharges and making uses of the NTSF reference nutrients data set of 1985 provided by the North Sea Task Force guidance document (Rijkswaterstaat, 1992) and amended proportionally with year-to-year variation of river discharge flow-rate. Initial conditions for ecosystem state variables were obtained by performing a “spin-up” simulation for the previous year with the above mentioned boundary conditions.

4 RESULTS AND DISCUSSION

4.1 Improved knowledge of the eutrophication process in the Belgian coastal waters

4.1.1 Nutrient enrichment status of BCZ

The present-day average nutrient enrichment of BCZ and its recent trends was estimated based on winter nutrient concentrations and salinity data collected since 1974. BCZ is a highly dynamic system with waters resulting of the mixing between the in-flowing Atlantic waters and freshwater inputs from the IJzer, Scheldt and Rhine rivers. As suggested by model simulations with 3D-COHSNS (section 3.2.1; K. Ruddick et al., 2003), the geographical extent of the river plumes varies mainly as function of wind, with tidal effects giving smaller scale modulations. The wind is in turn related to the NAO index (Marschal et al., 1997). Overall the nutrient enrichment in BCZ reflects the cumulative inputs from atmospheric and direct sources, Scheldt, IJzer and Rhine rivers, local benthic remineralization and the in-flowing Atlantic waters themselves enriched by nutrient loads by the river Seine and Somme. In order to encompass the changing hydrodynamics, the nutrient enrichment was best determined as nutrient concentrations extrapolated at the BCZ long-term average salinity of 33.5 (Rousseau, 2000; Rousseau et al. 2003).

Fig. 5-A shows the evolution of the average enrichment in NH_4 , $\text{NO}_3 + \text{NO}_2$, DIN, PO_4 and DSi (dissolved silicic acid) over 1974-2001. No significant change in DIN concentration (in average 29 μM) is observed over the period (Fig. 5-A). DIN evolution mostly reflects trend of $\text{NO}_3 + \text{NO}_2$ which account for ca 90% of N form in BCZ (Fig. 5A). A slight decrease of NH_4 concentrations is recorded since the mid-1980's and accelerates in 1998. DSi decreased slightly but significantly ($p < 0.05$) (Fig. 5-A). Most spectacular is the decreasing trend in PO_4 concentration ($p > 0.005$) from $\sim 2\mu\text{M}$ in 1974-1984 to $0.8\mu\text{M}$ in 2001 (Fig. 5-A).

The contrasted changes in PO_4 and DIN winter concentrations (Fig. 5A) were altering the N:P:Si balance of nutrients since 1974. The ecological importance of this change can be appraised in Fig. 5-B which compares the trends in DIN: PO_4 , DIN:DSi and DSi: PO_4 molar ratios of winter nutrients over the 1974-2001 period with average nutrient requirements of coastal phytoplankton (Redfield et al., 1963) and diatoms (Brzezinski, 1985). One major observation is the marked shift of N:P ratios from values closed to Redfield ratio during the 1972-1985 period to N excess conditions after the mid-1980's. The largest changes were observed during the 1990's when DIN: PO_4 increased from values around 20 to more than 30 since 1997. This suggests that PO_4 is nowadays the nutrient limiting phytoplankton growth in BCZ. On the other hand the interannual evolution of DIN:DSi and DSi: PO_4 molar ratios shows

that DIN availability largely exceeded the DSi requirement of diatom during the whole period (Fig. 5-B). The evolution of DSi: PO₄ ratio clearly suggests DSi limitation of diatom growth in central BCZ during the 1974-2001 period (Fig. 5-B). However, since the mid-1990's, the coastal system looks more balanced with respect to DSi and PO₄. Interestingly, the long-term trends of the global nutrient enrichment of BCZ (Fig. 5-A) are reflecting the evolution of Scheldt nutrient loads (Rousseau et al., 2003) especially NH₄ and PO₄. Observed PO₄ decrease is however much less pronounced at sea than in the Scheldt estuary where it drops by a factor 7. The role of alternate P sources such diagenetically remineralised P in such shallow waters or those associated to P-enriched Atlantic in-flowing waters together with the complex biogeochemistry of P could explain the observed discrepancy in P reduction.

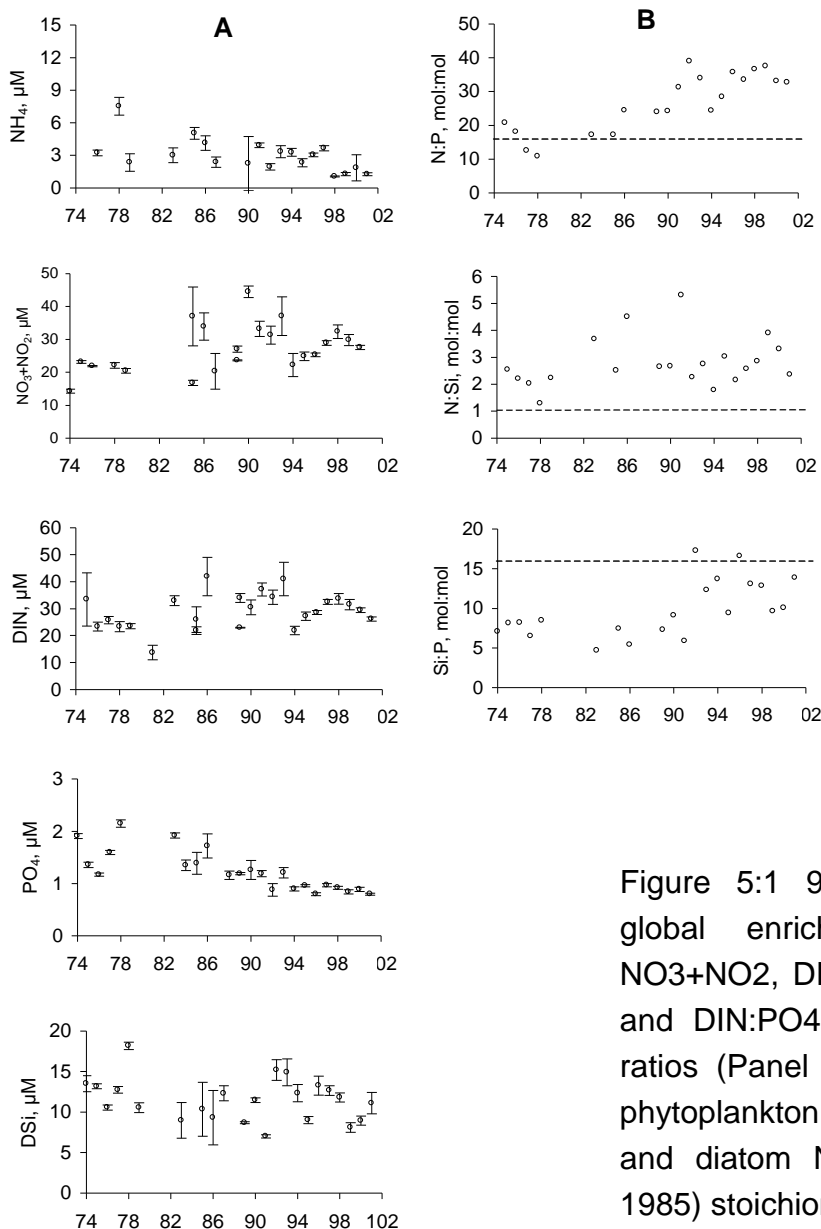


Figure 5:1 1974-2001 evolution of the global enrichment of BCZ in NH₄, NO₃+NO₂, DIN, PO₄ and DSi (Panel A) and DIN:PO₄, DIN:DSi, DSi:PO₄ molar ratios (Panel B). Hatched line indicates phytoplankton N:P (Redfield et al., 1963) and diatom N:Si and Si:P (Brzezinski, 1985) stoichiometry.

4.1.2 Response of phytoplankton blooms to nutrient enrichment

4.1.2.1 Diatom-*Phaeocystis* colony successions

Seasonality and recurrence are the most striking features of phytoplankton blooms recorded in the central BCZ (Station 330) during period 1988-1999 (Fig. 6). The seasonality is reflected by the level of Chl a concentration reached (Fig. 6a): a well pronounced spring outburst followed by further fluctuating summer and fall accumulations before reaching the winter level in mid-November, at the end of the vegetative season. These characteristics are also visible in the C-biomass pattern of the two main phytoplankton community components, the diatoms and *Phaeocystis* colonies (Fig. 6b, c). One single short-living bloom of *Phaeocystis* colonies occurs repetitively during spring after a first diatom growth. Diatoms are present throughout the vegetative period including that of *Phaeocystis* blooming (Fig. 6b, c) and are the main phytoplankters in early-spring, summer and fall (Fig. 6b). TWINSpan statistical analysis (Hill, 1979) identified three major diatom assemblages on basis of their period of occurrence and dominance and allowed reconstruction of a typical phytoplankton seasonal cycle illustrated by Fig. 7b for 1995. As shown by this figure, the phytoplankton spring succession is initiated in late winter-early spring by a community composed of small colony-forming species *Thalassiosira* spp., *Skeletonema costatum*, *Thalassionema nitzschioides*, *Plagiogramma brockmannii*, *Asterionella glacialis*, *A. kariana*, *Melosira sulcata*, *Biddulphia* spp. and the larger *Coscinodiscus* spp. This community, here reported as DIA1, again blooms from the end of August until the end of October (Fig. 7b) where it usually contributes to more than 90 % of the diatom C-biomass. DIA1 is progressively replaced by an ephemeral diatom assemblage composed of *Chaetoceros* spp. (mainly the colonial *C. socialis*), and *Schroederella* sp. (Fig. 7b). DIA2 is invariably associated to the onset of the blooming of *Phaeocystis* colonies. Small forms of these latter are often found in the setae of *Chaetoceros* spp. A third diatom community (DIA3) blooms at the same time of *Phaeocystis* colonies (Fig. 7ab) and is essentially composed of larger diatoms *Rhizosolenia* spp., *Guinardia* sp. and *Cerataulina* sp. but largely dominated by *Guinardia* sp. The latter genus composes usually the whole bulk of summer diatoms from June to about mid-September.

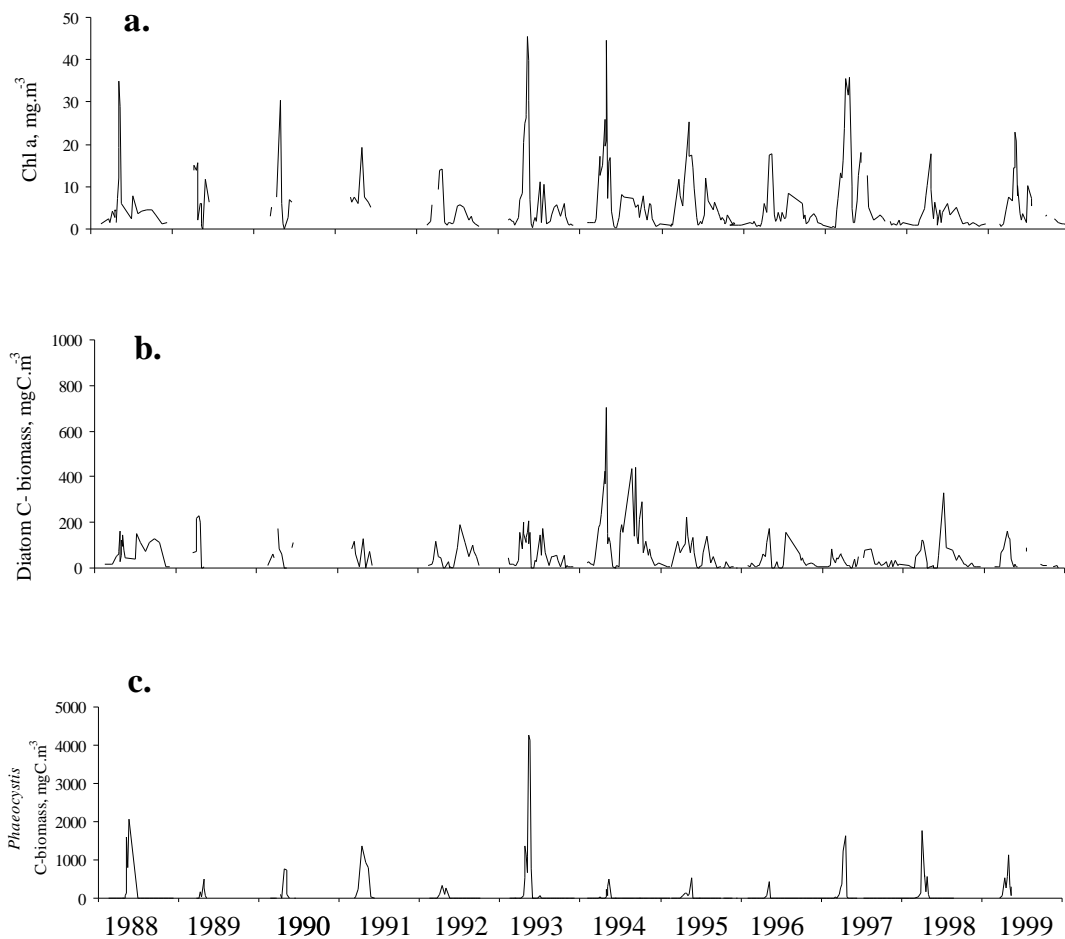


Figure 6: 1988-1999 evolution of a) Chl. a, b) diatoms and c) *Phaeocystis* colonies at station 330

4.1.2.2 Control of diatom and *Phaeocystis* colony blooms

While the phytoplankton seasonal succession of Fig.7A is remarkably repeated since our early observations in 1988, a significant interannual variability is observed in the timing, duration and magnitude of phytoplankton blooms (Figs. 6, 8). In spite of considerable progress we still don't have a complete understanding of the factors controlling the extent of the early spring diatom blooms as well as those regulating the relative magnitude of the co-occurrent *Phaeocystis* colonies and *Guinardia* sp. The success of a species can be due to a better ability for using the available resources (bottom up factors) and/or resistance to mortality (top down). Progress achieved on knowledge of bottom up – top down regulation of these blooms is described below.

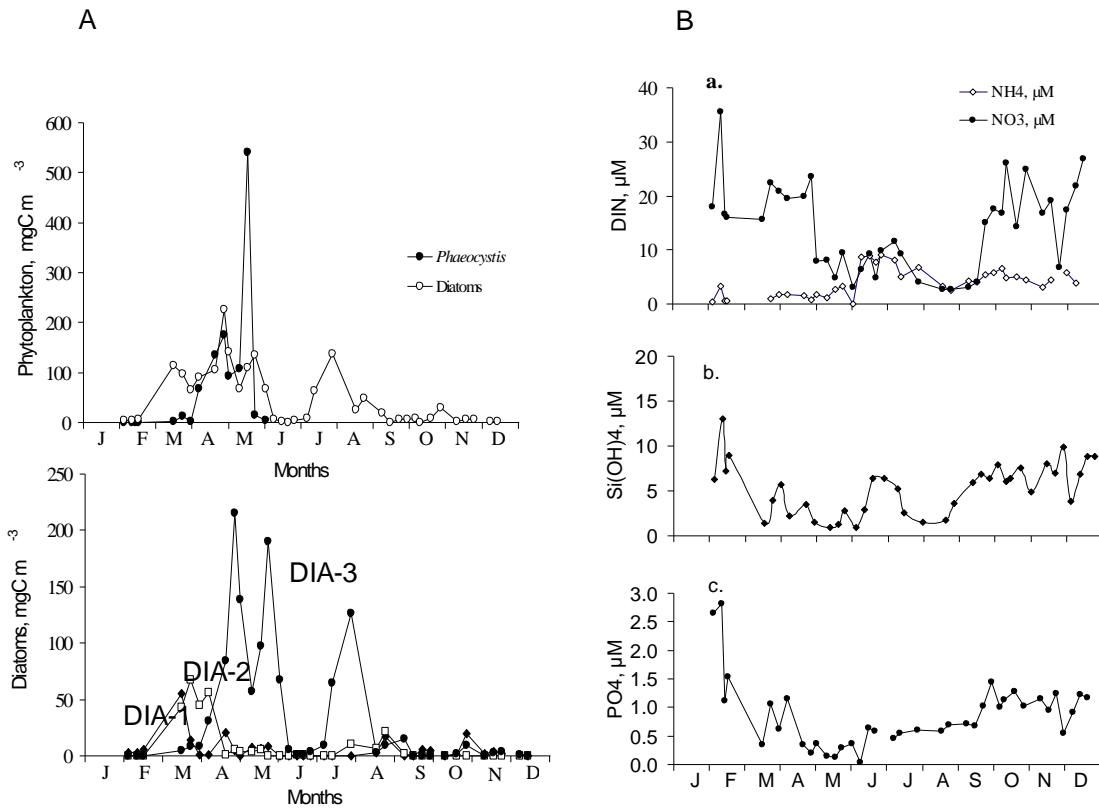


Figure 7: Seasonal changes of phytoplankton (Panel A) and inorganic nutrients (Panel B) recorded at station 330 of the Belgian coastal waters in 1995.

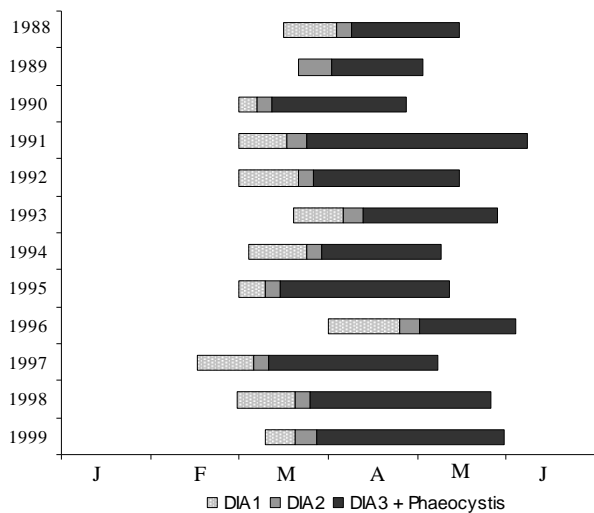


Figure 8: Timing and duration of the 3 main spring communities: DIA1, DIA2 and the assemblage of DIA3 and *Phaeocystis* colonies

Bottom-up

Bottom-up factors include light, temperature and nutrients. Considerable progress has been achieved in understanding their relative role in the control of phytoplankton successions in the Belgian coastal waters. Evidence now exists that a light threshold

of $\sim 12 \mu\text{mole m}^{-2} \text{s}^{-1}$ in the water column is required for the onset of the spring succession (Table II). Interestingly, this seasonal shift in the inception time of the bloom doesn't alter but moves the whole phytoplankton spring succession (Fig.8). This light threshold is reached between mid-February and mid-March at varying water temperature (4 - 8.2 °C) and incident irradiance (253 - 597 $\text{Jcm}^{-2} \text{d}^{-1}$) and relies on physical processes determining the load of suspended matter (Table II). Physiologically, this light level corresponds to the light required by early spring diatoms for an optimised cell division rate (Meyer et al., 2000). As shown by previous work (Lancelot and coll., SSTC-Marine Impulse, final report), these early spring diatoms (DIA-1) are also better competitive compared to *Phaeocystis* at the low temperature of late-February early March (5-6°C). On the contrary, *Phaeocystis* colonies optimise their growth at higher temperature and light but are better flexible than diatoms sudden changes of light due to a faster xanthophyll cycling rate (Meyer et al.2000). It is therefore concluded that, in the absence of any other limitation, *Phaeocystis* colonies are able to outcompete early spring diatoms at the higher light intensity of April. On the other hand, difference in temperature adaptation could not be evidenced for *Phaeocystis* colonies and DIA-3. A possible difference in light adaptation has still to be investigated.

Table II: Interannual variations of temperature, salinity, global radiation and averaged PAR in the water column at the onset of the spring bloom.

Year	Temperature (°C)	Global Solar Radiation ($\text{J. m}^{-2}.\text{d}^{-1}$)	Averaged PAR in the water column ($\mu\text{mol}.\text{m}^{-2}.\text{s}^{-1}$)
1988	5.8	384	14
1989	-	-	-
1990	8.2	414	14
1991	6.0	377	13
1992	5.9	323	11
1993	6.0	597	12
1994	5.5	351	10
1995	8.0	323	10
1996	4.0	421	13
1997	4.0	253	12
1998	5.9	294	12
1999	7.0	573	14

Seasonal changes of nutrients exemplified by Fig. 7B for 1995 suggest that the magnitude of the early spring diatom bloom (Fig. 7A) is controlled by the availability of Si(OH)_4 and PO_4 indicating that in the presence of large excess of NO_3 (Fig. 7B) the growth of DIA-2, DIA-3 and *Phaeocystis* colonies is sustained by regenerated forms of P and Si (only diatoms).

The importance of silicium in regulating the succession of the three diatom assemblages recorded every spring in BCZ was assessed by comparing the silica content of the different diatom assemblages with ambient silicium. Our results indicate that the 3 diatom assemblages that succeed along the spring bloom are characterised by distinct silica stoichiometry with molar Si:C decreasing from 0.68 to 0.04. The distinct Si:C stoichiometry reflects both specific properties and environmental control. It seems plausible that the high ambient silicic acid of late winter and fall, in combination with sufficient NO_3 and PO_4 and low light and temperature lead to the early spring dominance of highly silicified DIA-1 in BCZ (Fig. 7). The pattern is more complex for the spring and summer diatom communities (DIA-2 and DIA-3) which grow under higher light and temperature but low Si(OH)_4 and PO_4 conditions (Figs. 7). Indeed high light and temperature associated to low Si(OH)_4 would decrease the diatom Si:C while an opposite effect would result from PO_4 depletion. However the occurrence of DIA-1 and DIA-3 at very different light and temperature conditions would preclude these environmental factors to control Si:C of these diatoms. The decrease of ambient Si(OH)_4 from 14.5 μM to a minimum of 1.3 μM (Fig. 7) suggests that silicic acid availability could control the diatom Si:C. The observed seasonal pattern of diatoms might be due in part to differences in their silica requirement. Accordingly, a positive relationship was observed between the diatom Si:C and ambient Si(OH)_4 (Fig 9). Our relationship (Fig 9) fits well with the general observation in the aquatic environment that diatom Si:C is related to Si(OH)_4 concentrations. Freshwater diatoms were shown to be much more heavily silicified than the marine ones (Conley et al., 1989), Si(OH)_4 in freshwaters being much higher than that of marine waters. Among marine diatoms, those growing in the Southern Ocean, where Si(OH)_4 concentrations as high as 80 μM are recorded, are characterised by a Si:C as high as 0.65 (Nelson and Smith, 1986). Although the nutrient limitation status of the coastal diatom communities was not assessed during this study, the positive relationship existing between Si:C of the different diatom communities and Si(OH)_4 availability suggests that the succeeding diatom communities in Belgian coastal waters are well adapted to their silicic acid environment. This has been particularly well documented for the genus *Guinardia* which composed the bulk diatom during late spring and summer (Fig 7; Lancelot et al., 1998). *Guinardia* spp. is known to form huge blooms of 400 10^3 cells l^{-1} in May-June in the English Channel (Grall, 1972; Sournia et al., 1987) and in the Bay of

Brest (Ragueneau et al., 1994) when Si(OH)_4 is low. In the Bay of Brest, the shift observed from the early spring diatom bloom dominated by *Thalassiosira* spp. to a *Guinardia*-dominated community was also related to silicic acid availability (Del Amo et al., 1997a). Furthermore, Del Amo et al. (1997b) showed the ability of the *Guinardia* to grow on remineralized Si(OH)_4 from sedimented early spring diatoms, suggesting that this diatom is particularly well adapted to take advantage of low Si(OH)_4 . Altogether, our results support the hypothesis that ambient Si(OH)_4 is an important factor for shaping the diatom succession in temperate coastal ecosystem.

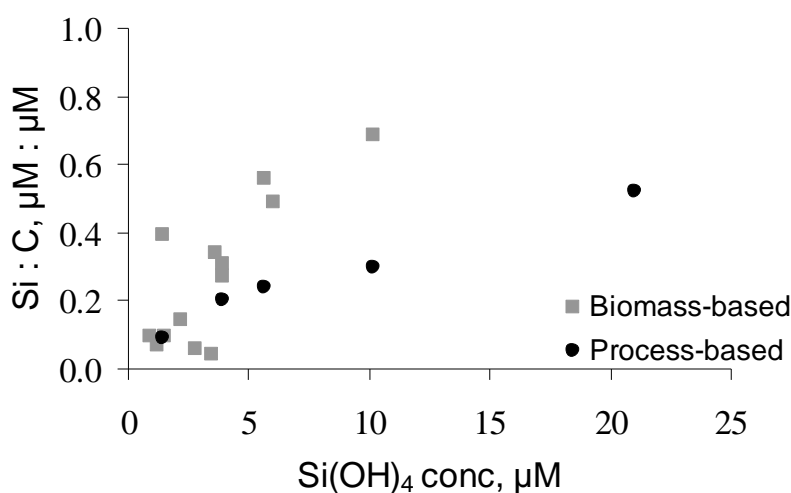


Figure 9: Relationship between the diatom Si:C ratio and ambient dissolved silicic acid from biomass- (filled circles) and process- (open circles) based measurements.

The role of NO_3 in regulating the magnitude of *Phaeocystis* colony blooms was evidenced by relating the maximum *Phaeocystis* cell density reached each year in different stations of the Southern Bight of the North Sea and the corresponding NO_3 left over at the time of DIA-1 decline (Fig.10; Lancelot, 1995; Lancelot et al., 1998). Under the low ambient PO_4 prevailing at the time of *Phaeocystis* colony blooms (Fig.), this relationship suggests that *Phaeocystis* growth is sustained by new sources of N but regenerated P. The ability of *Phaeocystis* cells to hydrolyze organically bound P under low PO_4 concentration has indeed been demonstrated (Veldhuis and Admiraal, 1987; Veldhuis et al., 1991). For the first time, PO_4 limitation was demonstrated in BCZ based on the measurement of alkaline phosphatase activity. One major result is that this enzymatic activity is associated to mainly large particles including phytoplankton cells and their attached bacteria. The highly significant correlation between alkaline phosphatase activity and *Phaeocystis* (Fig. 11) suggests that the colonies play a major role in PO_4 regeneration and are cleaving

organic phosphate for their own utilisation, hence competing with bacteria for phosphate uptake during this period of low ambient phosphate. Further investigations making use of specific probes for locating alkaline phosphatase on cell membrane are further required for absolutely stating on the mixotrophy ability of *Phaeocystis*. This is of prime importance for planning nutrient reduction policies.

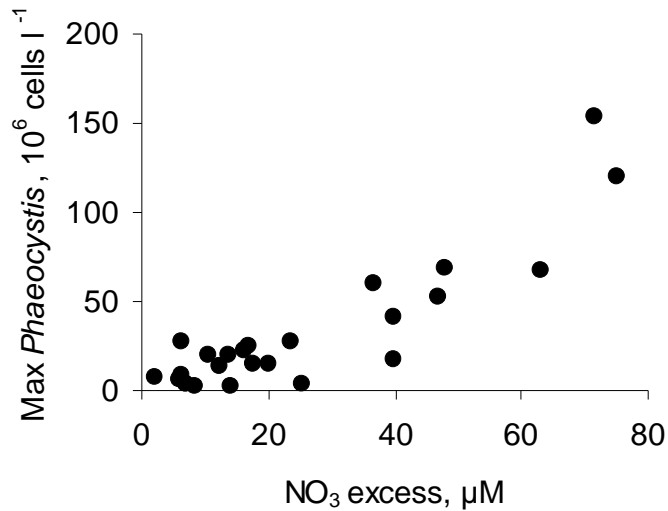


Figure 10: Relationship between maximum *Phaeocystis* cell density reached at several stations in the Southern Bight of the North Sea and excess NO₃

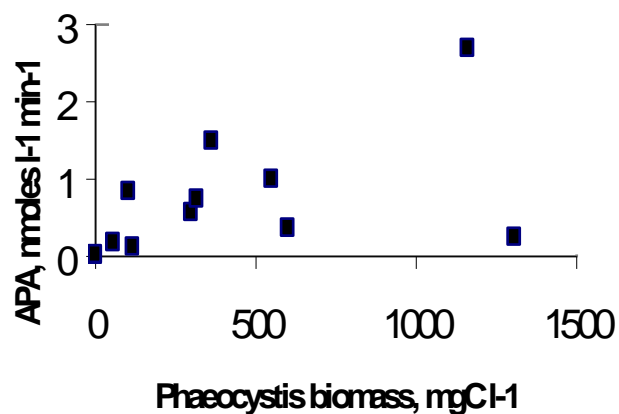


Figure 11: Relationship between alkaline phosphatase activity and *Phaeocystis* colony biomass (BCZ, Spring 1998; S. Becquevort, unpublished data).

Top-down

The pigment-empty guts of copepods shown in spring 1998 at the time of *Phaeocystis* colony blooms (Fig. 12; Gasparini et al., 2000) lead to believe that *T. longicornis*, the dominant copepod in spring, does not feed on colonies and so indirectly contributes to the successful extent of *Phaeocystis* colony blooms. Colony organisation and the skin like structure of the colony have been recently suggested to protect *Phaeocystis* colonies against copepod grazing but the nature of mechanisms other than increase in size was not specified. Based on these grazing experiments, Gasparini et al.(2000), hypothesised that adult copepods might be in food shortage if not starving during *Phaeocystis* blooms, which could impact negatively the next copepod generation. Additional data comparing ingestion rates based on phytoplankton cells counts with those estimated from egg production by field copepods collected in 2001 (Fig.13; E. Antajan, unpublished data) suggest that *T. longicornis* is not as such negatively affected by *Phaeocystis* colony blooming and necessarily feeds on other prey such as microzooplankton and *Phaeocystis*-derived particles. Interestingly enough phytoplankton is neither sufficient to fulfill copepods needs except during the winter season (Fig.13).

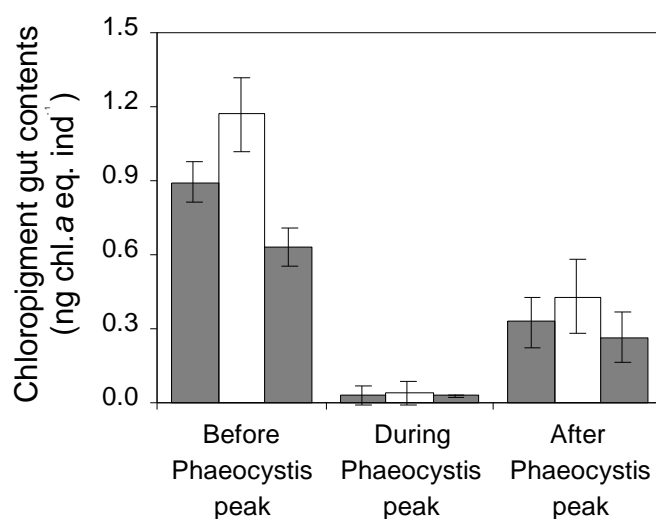


Figure 12: Averaged day-night values (\pm standard errors) of chloropigment gut contents measured in adults and late copepodite stages of *Acartia clausi* (hatched bars), *Centropages hamatus* (white bars) and *Temora longicornis* (dotted bars), before, during and after the *Phaeocystis globosa* peak in 1998 spring.

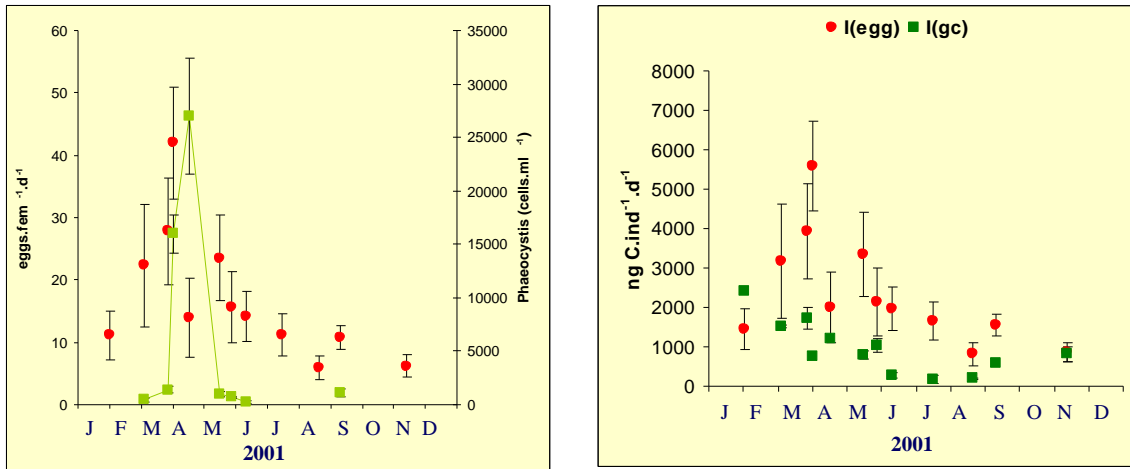


Figure 13: 2001 seasonal evolution of a) copepod eggs production and *Phaeocystis* colonies (in green) and b) copepod ingestion rates estimated from egg production and gut content. E. Antajan, unpublished data.

Finally our observations show that spring mesozooplankton include large numbers of gelatinous zooplankton such as *Pleurobrachia*, *Noctiluca* and *Oikopleura*. Whereas it has been shown that *Noctiluca* eats unicellular *Phaeocystis* and small colonies, nothing is known about the feeding characteristics and trophic significance of other gelatinous species with respect to *Phaeocystis* blooms.

4.1.3 Fate of ungrazed *Phaeocystis*-derived organic matter

4.1.3.1 Spring C budget and trophic efficiency of the planktonic food web

Fig.14 shows the carbon budget constructed on the basis of rate and biomass measurements performed at station 330 in spring 1998 during the *Phaeocystis* bloom event. The results are extensively described in Rousseau et al. (2000). The structure of the flow network shown on Fig.14 was designed based on the current knowledge of the trophic interactions between the main auto- and hetero-trophic planktonic organisms. These latter were therefore grouped according to their trophic position. So, phytoplankton was sorted as three trophodynamic groups with different trophic fates: *Phaeocystis* colonies, nanophytoplankton and diatoms. Diatoms feed mesozooplankton or are exported to the sediment solely or through aggregation. *Phaeocystis* colonies which resist grazing by mesozooplankton (Gasparini et al.,

2000) either sink or disrupt releasing in the water column dissolved organic matter and free-living cells. These latter cells are included in the bulk of nanophytoplankton composed of unidentified autotrophic flagellates. Nanophytoplankton is grazed by microzooplankton but do not sink due to its small size and low density. Products of organism lysis or *Phaeocystis* matrix dissolution supply the dissolved organic matter pool available to bacteria and so initiates a microbial network in which bacteria are grazed by nanoprotozooplankton, being themselves a food item for microzooplankton. In this model, microzooplankton is composed of various nanograzers, which include the usual microprotozooplankton (the protists: ciliates and dinoflagellates) but also small metazoans such as copepod nauplii, copepodites I-II and pluteus larvae. Altogether these organisms constitute a food resource for mesozooplankton here mainly composed of copepods.

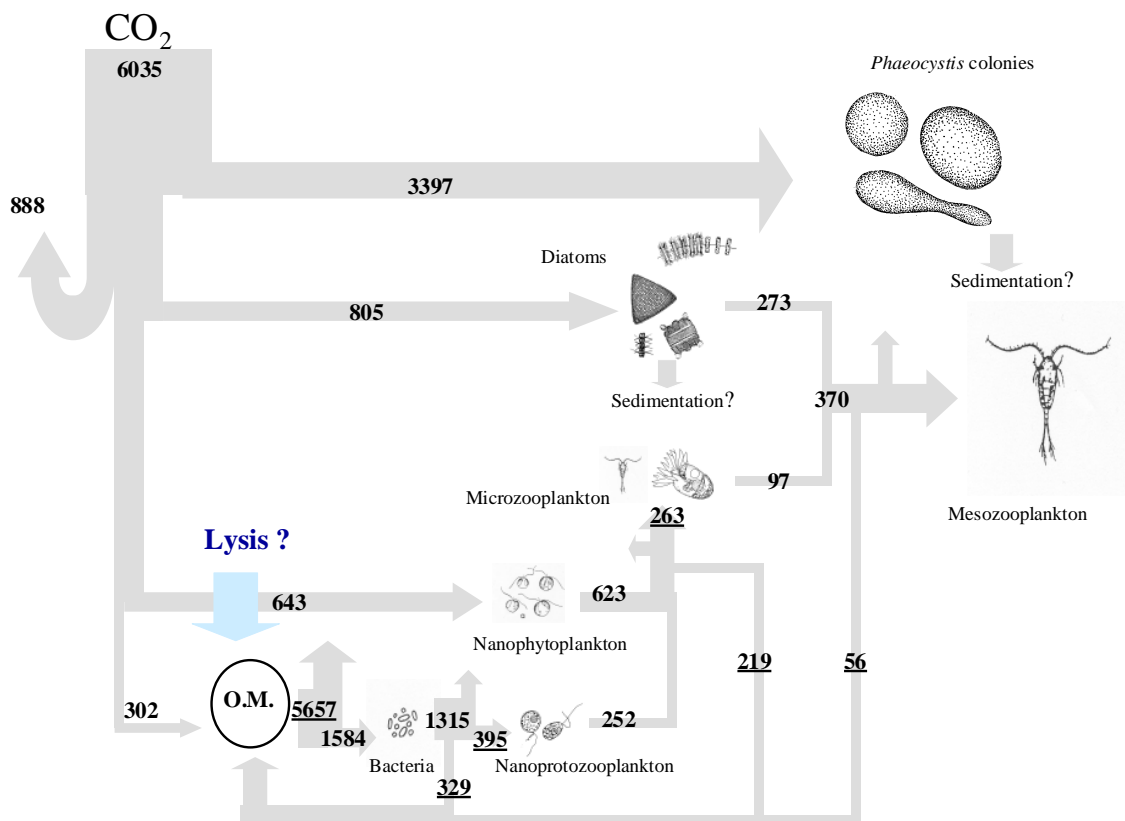


Figure 14: Spring carbon budget 1998 established on the basis of field rate measurements at Station 330. Flows are expressed in $\text{mgC m}^{-3} \text{ period}^{-1}$. Underlined figures correspond to calculated metabolic flows. OM represents the pool of organic matter.

As shown by Fig.14, a total of 6035 mgC m^{-3} was photosynthesised during the Diatom-*Phaeocystis* blooming period (105 days in 1998) by the 3 groups of phytoplankton. From this, 15 % was respired and 5 % was directly excreted as small metabolites. Some 70 % of the spring net primary production ($4846 \text{ mgC m}^{-3} \text{ period}^{-1}$) was attributable to *Phaeocystis* colonies while spring diatoms and nanophytoplankton contributed respectively 17 % and 13 %. As *Phaeocystis* colonies were not grazed by mesozooplankton, most of the net spring primary production escaped the linear food chain. Some $273 \text{ mgC m}^{-3} \text{ period}^{-1}$, i.e. one third of the net diatom production (Fig. 14), fuelled directly the mesozooplankton and contributed 74 % of the total mesozooplankton ingestion. The rest of the mesozooplankton diet was provided by the microbial food web through the grazing of mesozooplankton on microzooplankton ($97 \text{ mgC m}^{-3} \text{ period}^{-1}$). This transfer represented 37 % of the total production of the microbial food web ($263 \text{ mgC m}^{-3} \text{ period}^{-1}$; Fig. 14). This production issued from two distinct pathways corresponding to the production path of two possible prey items for microzooplankton. A direct one by the grazing of microzooplankton on nanophytoplankton and a more complex one on nanoprotozooplankton which biomass production relies on bacterial production (Fig. 14). Assuming no food selectivity, budget calculation of Fig. 14 shows a higher efficiency of the direct pathway nanophytoplankton-to-microzooplankton supplying 71 % ($623 \text{ mgC m}^{-3} \text{ period}^{-1}$) of the total microzooplankton diet ($875 \text{ mgC m}^{-3} \text{ period}^{-1}$). This flow corresponded to a transfer of 97 % of the nanophytoplankton production to higher trophic levels, suggesting a close coupling between microzooplankton and nanophytoplankton (Fig. 14). A lower proportion (64 %) of the nanoprotozooplankton production was ingested by microzooplankton, supplying 29 % of their needs. The nanoprotozooplankton was fuelled by bacterial production. The well-balanced budget between bacterial production ($1584 \text{ mgC m}^{-3} \text{ period}^{-1}$) and the nanoprotozooplankton grazing ($1315 \text{ mgC m}^{-3} \text{ period}^{-1}$) indicates a strong coupling between bacteria and their grazers. The bacterial carbon demand was estimated to $5657 \text{ mgC m}^{-3} \text{ period}^{-1}$. The autogenic sources of carbon for planktonic bacteria originate from phytoplankton exudation, lysis of auto- and hetero-trophic organisms and zooplankton egestion. Budget calculation shows that in 1998, the direct production of small substrates by phytoplankton amounted to $302 \text{ mgC m}^{-3} \text{ period}^{-1}$, i.e. 5 % of the bacterial needs. Zooplankton egestion contributed with $603 \text{ mgC m}^{-3} \text{ period}^{-1}$, i.e. about 11 % of the bacterial carbon demand (BCD). Together these two processes represented therefore a minor contribution to the BCD. Ungrazed *Phaeocystis* colonies, diatoms and nanophytoplankton amounted to 3397, 532 and $20 \text{ mgC m}^{-3} \text{ period}^{-1}$ respectively. Assuming a complete lysis of ungrazed primary production, autogenic carbon available for bacteria could amount to $4854 \text{ mgC m}^{-3} \text{ period}^{-1}$ which compares very well with the estimated BCD, $5657 \text{ mgC m}^{-3} \text{ period}^{-1}$

although not sufficient. The discharge of continental organic matter by the river Scheldt should therefore be considered as a complementary source of biodegradable in BCZ. Still our results suggest that disruption and dissolution of ungrazed *Phaeocystis* colonies might be the major process stimulating the bacterial activity in the Belgian coastal waters.

The spring carbon budget of Fig.14 suggests that the trophic efficiency of the planktonic food web is very low in the *Phaeocystis*-dominated BCZ. In spite of its major contribution to mesozooplankton feeding, the trophic efficiency of the linear food chain, defined as the ratio between mesozooplankton grazing on diatoms and diatom biomass production, was only 34 %. It is lowered to 5.6 % if the total available net primary production is considered. The trophic efficiency of the microbial food chain was calculated as the ratio between mesozooplankton grazing on microzooplankton and the resource inflow. The latter corresponded to the sum of the bacterial carbon demand and the nanophytoplankton production. This calculation gives a trophic efficiency of 1.5 % suggesting that the transfer of carbon to mesozooplankton through microzooplankton grazing was not significant.

Altogether these carbon-based calculations suggest that most of the *Phaeocystis*-derived production is remineralised in the water column and does not reach the sediment. Although no direct sedimentation of *Phaeocystis* material has been measured in BCZ, this result contrasts with visual observation (A. Cattrijsse, unpublished) and sediment spring release of dissolved Mn and Fe recorded in spring in BCZ (Schoemann et al., 1998) as indirect measurement of spring transfer of fresh organic matter from the water column to the sediment. Also puzzling is the apparent contradiction between the calculated complete remineralization of *Phaeocystis*-derived organic matter in the water column and the observed foam accumulations observed every spring on the beaches bordering BCZ (Lancelot, 1995). Both questions are addressed in the following sections.

4.1.3.2 Origin and biodegradability of dissolved organic carbon in BCZ during the wax and wane of *Phaeocystis* bloom

The allochthonous vs autochthonous origin and biodegradability of dissolved (DOC) and particulate (POC) organic carbon in BCZ was investigated in May 1999 at the time of *Phaeocystis* bloom. A serie of microbial assays were run on water samples collected at different location along a Scheldt estuary-Belgian marine waters gradient. Particulate attention was paid to the saccharidic (mono & poly) fraction of DOC due to the polysaccharidic nature of the *Phaeocystis* colony matrix. Results obtained (Fig. 15) establish the autochthonous and *Phaeocystis* origin of

biodegradable DOC (BDOC) in BCZ. The autochthonous origin is first suggested by the tremendous accumulation of autochthonous DOC of 60-110 $\mu\text{M C}$ composed of about 30 % of dissolved saccharidic-C (DTCHO) which contrasts with the conservative behaviour relative to ideal dilution of terrestrial DOC brought by the Scheldt (Fig. 15). Also, the major (80%) polymeric composition of the accumulated sugars in the coastal waters (Fig.16) suggests a recent release of the accumulated DOC in the marine waters. The comparable order of magnitude between accumulated DOC and the average maxima of *Phaeocystis* colony bloom recorded in BCZ (Rousseau, 2000), argues for a *Phaeocystis* origin of the DOC accumulation. Moreover, the high biodegradability of the bulk of the accumulated DTCHO in the marine area (Fig. 15 Pannel B) provides indication that polysaccharides released in the surrounding medium after *Phaeocystis* colony disruption are potentially very labile. This biodegradable DTCHO represents 45- 90% of biodegradable DOC in the marine area indicating that other biodegradable molecules such as for instance peptides are released in the surrounding medium after *Phaeocystis*-colony disruption and cell lysis. Additional time-course experiments show that the bulk of BDOC and BPOC is very rapidly degraded (within 3 days; Déliat et al., 2003; C. Leblanc unpublished data). However the very low bacterial growth efficiency of 8-10% measured along these microbial assays (Déliat et al., 2003) suggest that most of the carbon taken up is respired, probably due to PO_4 shortage at this period of the year (Fig.8). This result gives additional support to the very low efficiency of the microbial food chain concluded from the planktonic carbon budget previously established by Rousseau et al. (2000).

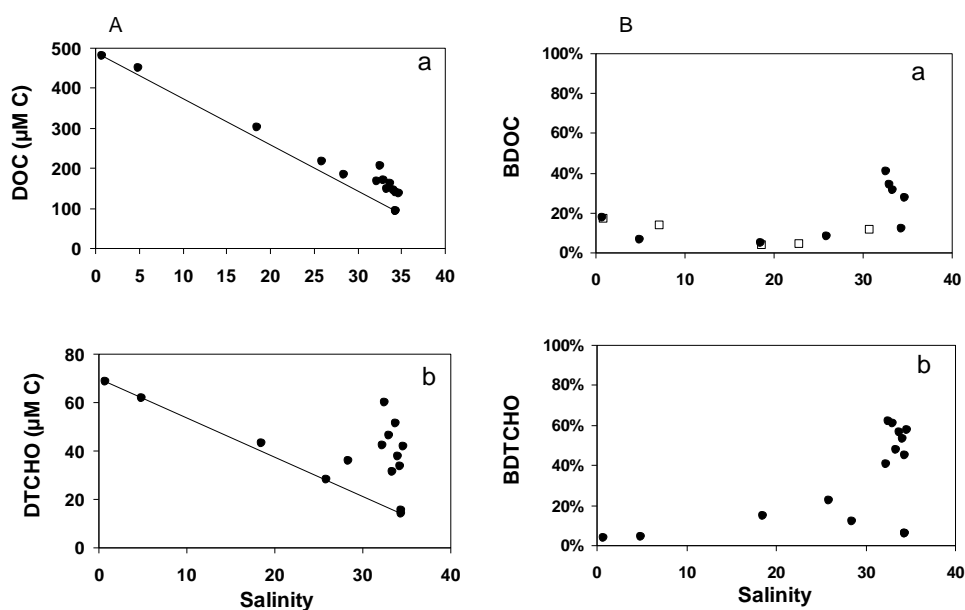


Figure 15: Salinity gradient of total (Pannel A) and biodegradable (Pannel B) dissolved organic carbon and sugars in May 1999.

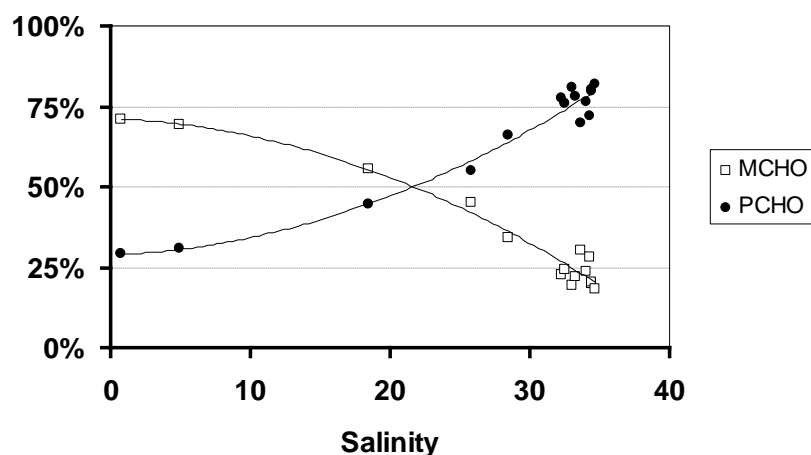


Figure 16: Mono-(MCHO) vs poly-(PCHO) fraction of dissolved sugars along the salinity gradient in May 1999.

4.1.3.3 Potential sinking rate of phytoplankton-derived particles

For the first time in BCZ, the potential sedimentation of phytoplankton and derived aggregates was measured using SETCOL sedimentation columns (SETCOL, Bienfang 1981). The obtained potential sinking rates of Chl a-related particles (C. Leblanc, unpublished data) were shown to vary between 0.1 and 6 m d⁻¹ with the highest rates (3 - 6 m d⁻¹) near shore in the area of maximum suspended matter. Comparable rates were obtained under laboratory-controlled conditions with pure cultures of the diatom *Asterionellopsis glacialis* (DIA-1) and senescent *Phaeocystis* colonies. On an average, the potential sinking rates of *A. glacialis* and *Phaeocystis* colonies and their derived aggregates were very comparable (~2m d⁻¹; C. Leblanc, unpublished data). Interestingly enough, values as high as the maximum potential rates measured in the field (6 m d⁻¹) were only obtained with senescent *Phaeocystis* colonies and aggregates (5-8 m d⁻¹; Fig. 17). Fig. 17 also indicates that the potential sinking rate of *Phaeocystis* colonies and derived aggregates varies according to the size of the particle with positive sinking rate at diameter <270 µm and on the contrary ascending rate for particles >270 µm. Maximum potential sinking rates were measured for *Phaeocystis* size-class between 150 and 250 µm. Finally, for each chosen size-class, the potential sinking rates of *Phaeocystis* aggregates were always higher than that of colonies (Fig. 17). We then conclude that the transient nature of *Phaeocystis* aggregation currently observed in BCZ (Becquevort et al., 1998) might result of the combined effect of a high sinking rate of *Phaeocystis*-derived particles, in combination with a high biodegradability and dissolution of *Phaeocystis*-derived material as shown in 3.1.3.2.

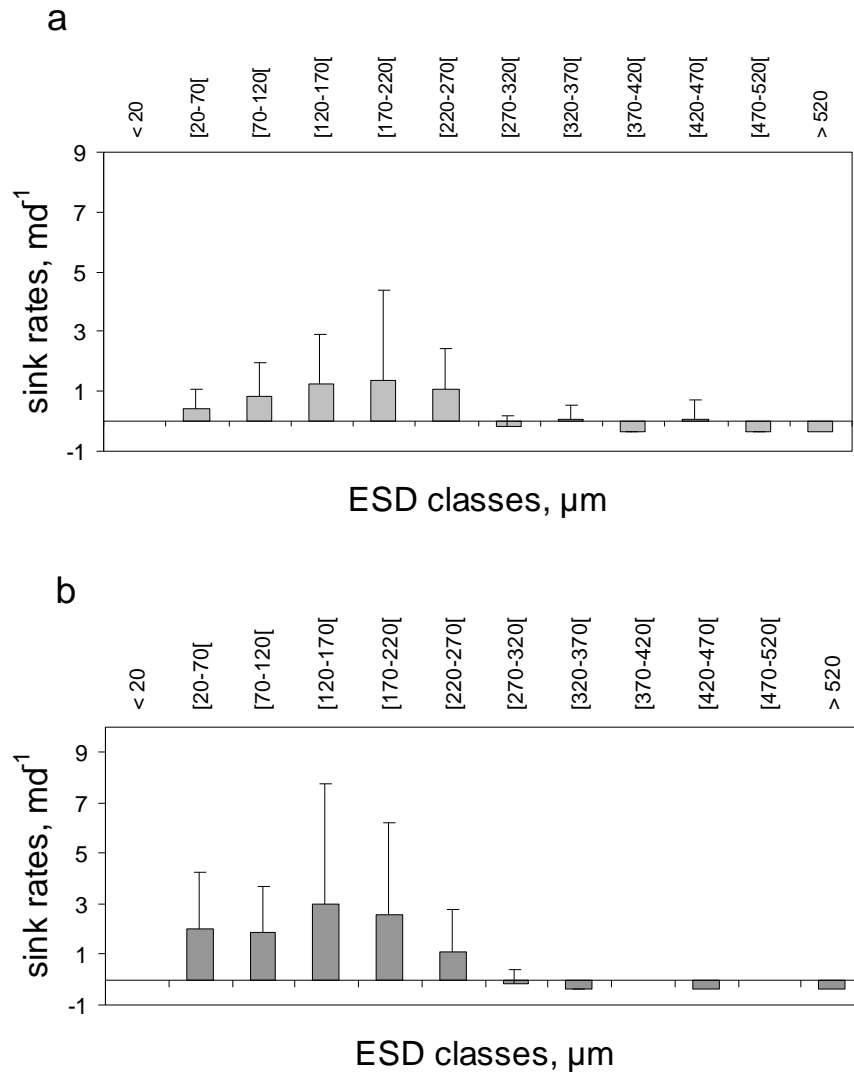


Figure 17: Potential sinking rates of a) *Phaeocystis* colonies and b) their derived aggregates sorted according to the size. ESD: Equivalent Spheriacle Diameter. C. lebank, unpublished data.

4.2 Modelling *Phaeocystis* blooms in BCZ

Numerical experimentation in AMORE aims at implementing MIRO&CO, a 3D biogeochemical model simulating the transport and dynamics of nutrients, spreading of diatom and *Phaeocystis* blooms in the Southern Bight of the North Sea and their impact on ecosystem structure and function. MIRO&CO results of the online coupling between the 3D-COHSNS hydrodynamic model (Ruddick et al., 2003) and the ecological model MIRO, previously developed and validated in a 0D multi-box frame (Lancelot et al., 2003).

The objectives of the ecosystem simulations carried out within AMORE are both scientific and environmental. Firstly, the use of an ecosystem model provided it is realistic, gives a very complete description in space and time of a large number of ecosystem quantities and processes as compared to the very sparse description that is available from field observation. Moreover, variation of parameters and boundary/initial conditions in sensitivity studies and comparative tests allows the key processes and the forcing factors that control them to be identified. For example, questions regarding the relative importance of top-down controls of phytoplankton from grazing by zooplankton against bottom-up control from nutrients, light and temperature can be investigated by numerical simulations with varying parameters sets. Secondly, the use of an ecosystem model can provide a scientific basis for environmental management by giving a response, albeit subject to the uncertainties of the model, to “what-if” questions such as nutrient reduction scenarios.

Progress gained by AMORE in 0D-MIRO and 3D-MIRO&CO are summarized below.

4.2.1 Upgrading and performance of the ecological model 0D-MIRO

4.2.1.1 Model structure and parameterisation

Fig.18 shows a schematic representation of the MIRO trophic structure. Thirty-two state variables (Table III) and twenty-six processes linking them were identified as important from the knowledge of the structure and functioning of *Phaeocystis*-dominated ecosystems. The model results of the integration of 4 modules describing the dynamics of phytoplankton (3 taxa), zooplankton (2 taxa), dissolved and particulate organic matter degradation and nutrient (NO_3 , NH_4 , SiO , PO_4) regeneration in the water column and the sediment (Fig. 18). State variables and processes parameterisation are fully described in Lancelot et al. (2003).

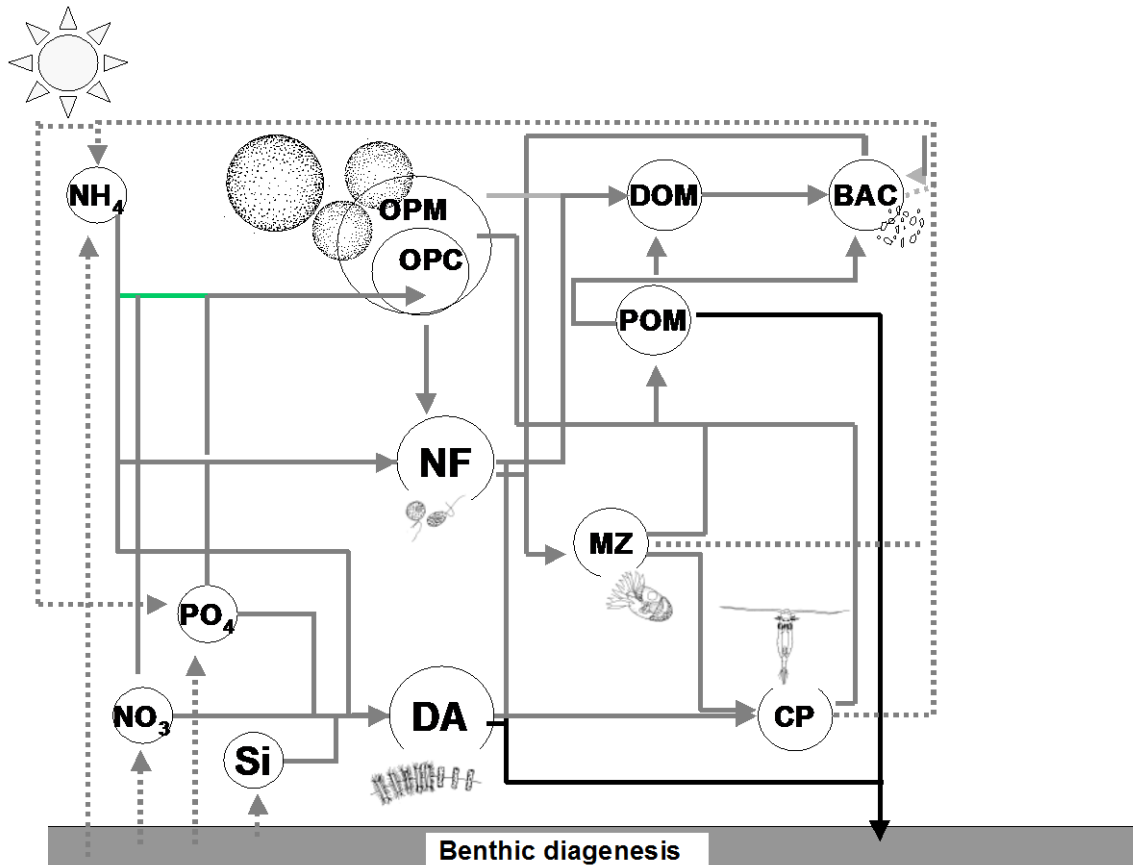


Figure 18: Structure of the MIRO model. Si: $\text{Si}(\text{OH})_4$; DA: diatoms; NF : nanoflagellates ; OPC : *Phaeocystis* colonial cells ; OPM : *Phaeocystis* colony matrix ; MZ : microzooplankton ; CP : copepods ; BAC : bacteria ; POM : Particulate organic matter ; DOM : dissolved organic matter.

Phytoplankton

The phytoplankton module considers 3 phytoplankton groups: diatoms (DA), free-living autotrophic nanoflagellates (NF) and *Phaeocystis* colonies (OP). Due to their trophic fate, *Phaeocystis* free-living cells and colonies are considered as separate state variables, even though they constitute two different stages of the life cycle of the same phytoplankton (e.g. Rousseau et al., 1994). *Phaeocystis* free-living cells are included in NF while colonies are described by the sum of two state variables [the colonial cells (OPC) and matrix (OPM)]. Phytoplankton growth is described according to the AQUAPHY model of Lancelot et al. (1991). This considers 3 intracellular pools - monomers (S); reserve material (R); functional and structural metabolites (F) - and distinguishes photosynthesis (directly dependent on light availability), from the process of growth controlled by the availability of intracellular monomers and ambient nutrients. A multiplicative function is used for describing the light and nutrient co-limitation but nutrient co-limitation is formulated as an additive function (O'Neill et al.,

1989). With respect to *Phaeocystis* colonies, an additional pool of ectopolymers (OPM) has been added to consider the mucilaginous colony matrix in which the cells are embedded and which serves as a reserve of energetic material (Lancelot and Mathot, 1985, Veldhuis et al., 1985). Beside respiration, common loss processes include excretion and cellular lysis, the latter function of nutrient stress. Taxon-specific losses include sinking rate (DA and OP) modulated by nutrient stress; grazing by microzooplankton (NF) and copepods (DA) and *Phaeocystis* colony disruption (OP). The latter process is indirectly related to nutrient stress being increased by a factor 10 when OPM is greater than OPF by a factor 1.7. Colony disruption partly forms aggregates and partly supplies free-living cells (NF) and labile dissolved organic carbon (DC1)

Zooplankton

The MIRO zooplankton module involves two groups of zooplankton: the microzooplankton (MZ) feeding on free-living autotrophic nanoflagellates (NF) and bacteria (BC) and the mesozooplankton (CP) grazing on diatoms (DA) and microzooplankton (MZ). *Phaeocystis* colonies are not subject to grazing (Breton et al. 1999; Gasparini et al., 2000). A simplified description of zooplankton dynamics has been chosen. The sigmoid (Holling III) function has been selected to describe the prey-dependence of zooplankton grazing. Two separate parameterisations are used to describe MZ grazing on NF and BC since heterotrophic nanoflagellate grazing on bacteria is not detailed explicitly in this version of MIRO. On the contrary, CP grazing is described by one unique Holling-III function of total preys (DA+MZ). No active selective feeding (food preference) is presently considered due to the lack of data and the current controversy about copepods preference for MZ or DA. Zooplankton growth and excretion are calculated from (grazing- egestion) rates based on growth efficiency, zooplankton stoichiometry and the stoichiometric composition of food. The model assumes thus that zooplankton excretes compounds with varying stoichiometry in order to maintain a constant body C:N:P. Second-order mortality (natural and predation by higher trophic levels) is considered for CP and constitutes the MIRO closure term.

Microbial loop

The degradation of organic matter by planktonic bacteria is described according to the HSB (High polymers, Small substrates and Bacteria) model of Billen (1989), considering two classes of biodegradability for both dissolved (DOM1 and DOM2) and particulate (POM1 and POM2) organic matter. The hydrolysis of these polymers produces dissolved monomers (BS) that can be taken up by bacteria. The ectoenzymatic hydrolysis of DOM is described by Michaelis-Menten kinetics. The

current version of MIRO uses first-order kinetics for POM hydrolysis with a temperature dependence of labile POM hydrolysis constant for considering the process-dependence on bacterial activity. According to their origin, C and N contribute in variable proportions to the pools of organic matter. This proportion, compared to the bacterial C:N ratio (assumed to be constant) determines whether net ammonification or ammonium uptake accompanies bacterial activity. All organic phosphorus is assumed to be released directly as PO_4 during hydrolysis of polymeric organic matter and P is taken up by bacteria in its inorganic form only. P uptake depends on the C:N composition of BS and is not dependent on ambient PO_4 provided its concentration is sufficient. With this assumption bacteria are more competitive than phytoplankton for low PO_4 .

Benthic diagenesis

Benthic organic matter degradation and nutrient (N, P, Si) recycling are calculated making use of the algorithms developed by Lancelot and Billen (1985) and Billen et al., (1989). These algorithms, by solving steady-state diagenetic equations expressing the mass balance of organic carbon, oxygen, inorganic forms of nitrogen and phosphorus in the sedimentary column, calculate the fluxes of nitrate, ammonium and phosphate across the sediment-water interface resulting from a given sedimentation flux of particulate organic matter. Furthermore, first-order kinetics describes benthic silicon dissolution and release of silicic acid to the water column. Particle adsorption of ammonium and phosphate are described by first-order equations and the coefficients are determined based on sediment porosity.

Table III The MIRO model biogeochemical state variables

Variable	Symbol
<u>Biological state variables:</u>	
Diatoms: DA= DAF+DAS+DAR	
Functional and structural metabolites	DAF
Monomers	DAS
Reserves	DAR
Phototrophic nanoflagellates: NF=NFF+NFS+NFR	
Functional and structural metabolites	NFF
Monomers	NFS
Reserves	NFR
<i>Phaeocystis</i> colonies: OP=OPF+OPS+OPR+OPM	
Functional and structural metabolite	OPF
Monomers	OPS
Reserves	OPR
Mucous matrix	OPM
Bacteria	BC
Microzooplankton	MZ
Copepods	CP
<u>Organic matter</u>	
Monomeric: carbon, nitrogen	BSC, BSN
Dissolved polymers (high biodegradability): carbon, nitrogen, phosphorus	DC ₁ , DN ₁ , DP ₁
Dissolved polymers (low biodegradability): carbon, nitrogen, phosphorus	DC ₂ , DN ₂ , DP ₂
Particulate organic matter (high biodegradability): carbon, nitrogen, phosphorus	PC ₁ , PN ₁ , PP ₁
Particulate organic matter (low biodegradability): carbon, nitrogen, phosphorus	PC ₂ , PN ₂ , PP ₂
Detrital biogenic silica	BSi
<u>Inorganic nutrients:</u>	
Nitrate	NO ₃
Ammonium	NH ₄
Phosphate	PO ₄
Silicic acid	SiO

4.2.1.2 Model implementation

For the application of the 0D-MIRO model to the continental coastal waters of the North Sea, a multi-box frame has been considered based on the hydrological regime. This simple resolution of the hydrodynamics represents a first approach to this tidally well-mixed area. In order to take into account the cumulated nutrient enrichment of Atlantic waters by the Seine and Scheldt rivers, two successive boxes (FCZ, BCZ), assumed to be homogeneous, have been chosen from the Baie de Seine to the Belgian coastal zone (Fig. 3). The offshore limit of the boxes is taken along a residual streamline so that inshore-offshore exchanges by residual advection can be neglected. Each successive box has its own characteristics (see Lancelot et al., 2003 for details) and is treated as an open system, receiving waters from the Southern adjacent box and exporting water to the Northern one. The seasonal variation of the state variables is calculated by solving the equations expressing mass conservation in the system with an Eulerian time discretisation. Climatological functions calculated from the period 1989-1999 are used for meteorological and river input forcing. These functions were parameterised from recorded daily solar global radiation (meteorological station Oostende, IRM) and seawater temperature, and monthly nutrient loads for the rivers Seine (Cellule Antipollution de Rouen du Service de la navigation de la Seine in France) and Scheldt [Institute for Inland Water Management and Waste Water Treatment (RIZA, The Netherlands) and Department of Environment and Infrastructure (Ministry of Flemish Community, Belgium)]. The latter are directly mixed at each time step (15 minutes) in the relevant boxes.

The South-Western (SW) boundary conditions are provided by the results of MIRO calculations performed for the conditions existing in the western Channel area (WCH), considered as a quasi oceanic closed system. For this application model runs are performed for meteorological conditions of 1989 until a steady state is reached. This occurs after 3 years.

4.2.1.3 Model results

Seasonal features of nutrients and phytoplankton blooms along the SW-NE gradient

The current capability of MIRO to reproduce the observed SW-NE nutrient enrichment gradient and the related spreading of phytoplankton blooms in spring is shown in Fig.19-20. These figures compare the climatological seasonal cycle of nutrients (Fig.19) and phytoplankton (Chl a and *Phaeocystis* cells; Fig.20) predicted by MIRO runs in the successive boxes WCH, FCZ and BCZ with 5 day-average data collected in 1989-1999 at 3 reference stations (WCH: 48°43.30N, 03°50W; FCZ: 50°44.5 N, 01°30.8E; BCZ: 51°26.05 N; 002° 48.50 E). As a general trend the

model reproduces fairly well for all nutrients the cumulated SW-NE nutrient enrichment shown by the three- (DSi, PO₄) to four- (NO₃) fold increase of winter concentrations in BCZ (Fig. 19a-c) when compared to the winter signature of the Atlantic waters (WCH; Fig. 19g-i). One exception is the MIRO overestimation of winter PO₄ in Atlantic waters (Fig. 19i). This can be explained by the lack of consideration of P retention in the sediment of box WCH. This overestimation, however, does not bias nutrient predictions in the successive FCZ (Fig. 19f) and BCZ (Fig. 19c). The timing and magnitude of spring nutrient decrease (Fig. 19) is also well represented by the model and corresponds with the phytoplankton spring development (Fig. 20). The Spring maximum Chl a predicted in each box corresponds reasonably well with observed average concentrations for the simulated 1989-1999 period and shows a four-fold increase along the SW-NE gradient (Fig. 20a,c,e). These maxima coincide with *Phaeocystis* blooms (Fig. 20b,d) except in the WCH where no *Phaeocystis* bloom is predicted by the model, in agreement with previous monitoring studies (Lancelot et al., 1987). As a general trend the modelled *Phaeocystis* cell abundance in FCZ and BCZ culminates some 5 days earlier than in the field and corresponds in magnitude to the highest observed concentrations and even more (Fig. 20b,d). Less well predicted in FCZ and BCZ are the summer nutrient decreases (Fig. 19) and phytoplankton blooms (Fig. 20a,c). The MIRO underestimate of summer-fall Chl a (Fig. 20a,c) likely explains the concomitant overestimate of nutrients (Fig. 19) suggesting that the dynamics of summer blooms is less well captured by the model compared to spring.

Seasonal distribution of auto- and heterotrophic biomasses and related biogeochemical variables in BCZ

The ability of MIRO to describing the dynamics of *Phaeocystis*-dominated ecosystems is shown in Fig. 21. This figure compares modelled seasonal distributions of auto- and heterotrophic biomasses and related biogeochemical variables in BCZ with observations collected at station 330 (51°26.05 N; 002° 48.50 E). The main ecological trends (temporal succession of auto- and hetero-trophic microorganisms, order of magnitude of biomass reached) and related nutrient cycles are reasonably well simulated considering the complexity of the ecosystem and the simplified physics used here. Particularly well simulated are the spring-summer phytoplankton successions with *Phaeocystis* colonies and nanophytoflagellates (Fig. 21b,c) blooming in between spring and summer diatom blooms (Fig. 21a). It has to be mentioned that the simulation of the observed summer diatom bloom (Fig. 5a) and related Si cycle (Fig. 21b) can only be obtained by attributing to diatoms two different parameter sets for temperature adaptation and Si:C stoichiometry according to the season. This corresponds to the observed shift from a high-silicified early-spring

diatom to a low-silicified summer population (Rousseau et al., 2002). Yet the obtained summer predictions correspond to the lower range of observed summer diatom biomasses (Fig. 21a) and are not reproducing the summer minima observed for all nutrients (Fig. 19a-c; Fig. 21g). The observed copepod spring-summer biomass is less well simulated due to a failure of the current version of MIRO to describe properly the copepod feeding function. As a consequence in our simulations the spring diatoms are not controlled by copepod grazing and most of spring diatom decrease is explained by sinking and lysis. The latter process release labile organic matter which stimulates bacterial growth at diatom decline (Fig. 21a, f). The predicted magnitude of spring bacterial biomass is significantly higher than observed (Fig. 21f) and can be explained by an underestimation of microzooplankton (Fig. 21e). According to our model, the diatom decline corresponds with lowest Si concentration (Fig.19b). *Phaeocystis* colony decline (Fig. 21c) on the other hand is associated with PO_4 minima (Fig.19c). This process releases labile DOC (Fig. 21h) and free-living cells (Fig. 21b). The latter stimulates microzooplankton growth (Fig. 21e) which in turn represses bacterial growth (Fig. 21f) permitting transient accumulation of labile DOC (Fig. 21h).

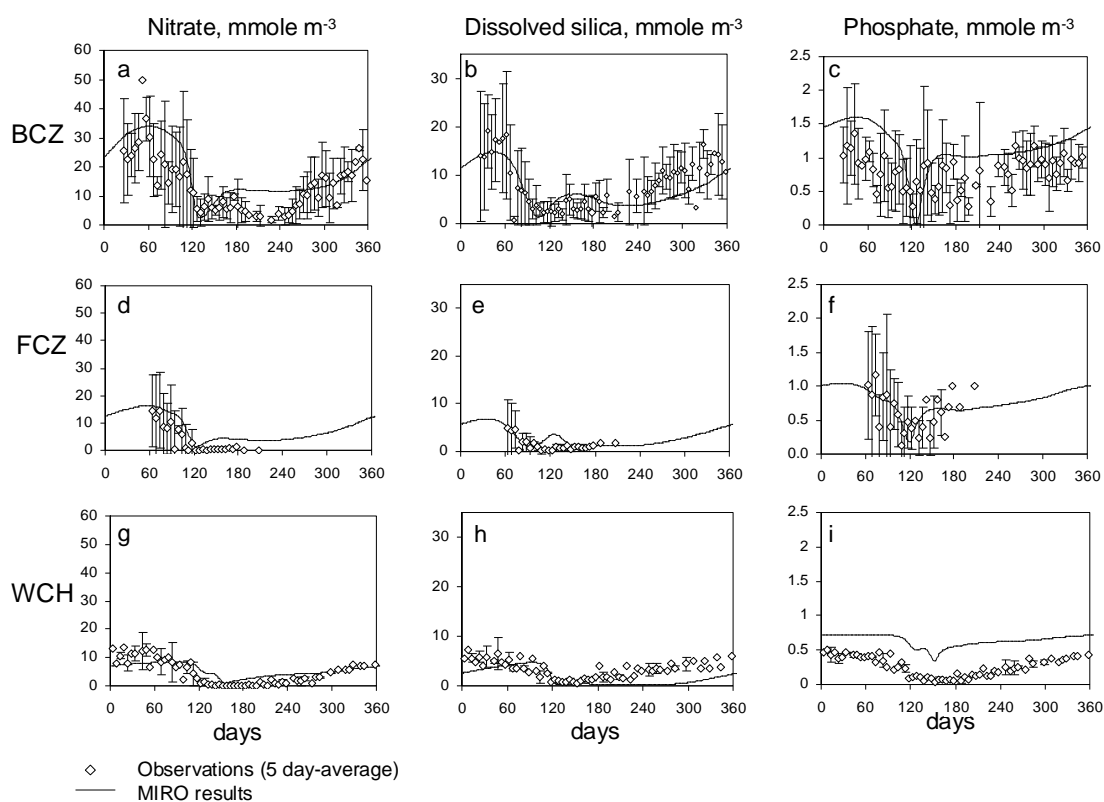


Figure 19: 0D-MIRO results (climatological run) and 1988-1999 available observations at 3 monitoring stations along the SW-NE gradient: Nutrients.

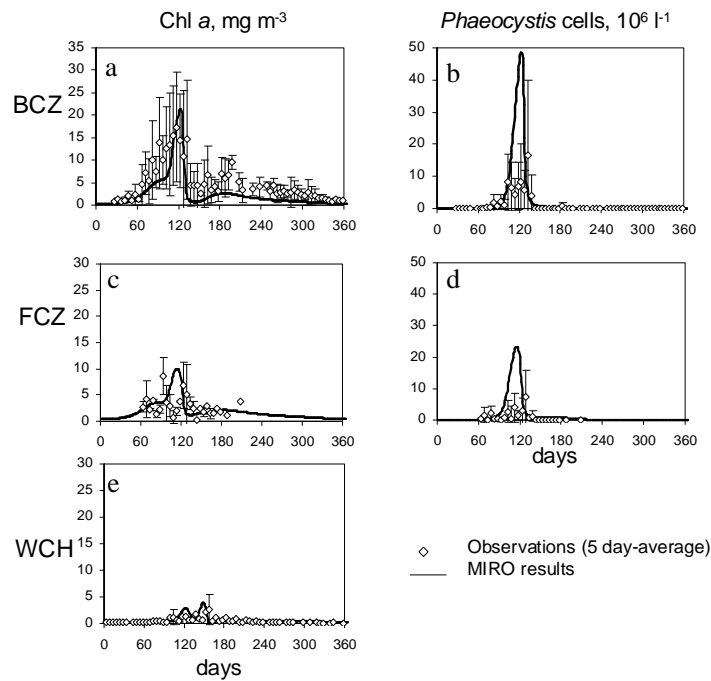


Figure 20: 0D-MIRO results (climatological run) and 1988-1999 available observations at 3 monitoring stations along the SW-NE gradient: Phytoplankton.

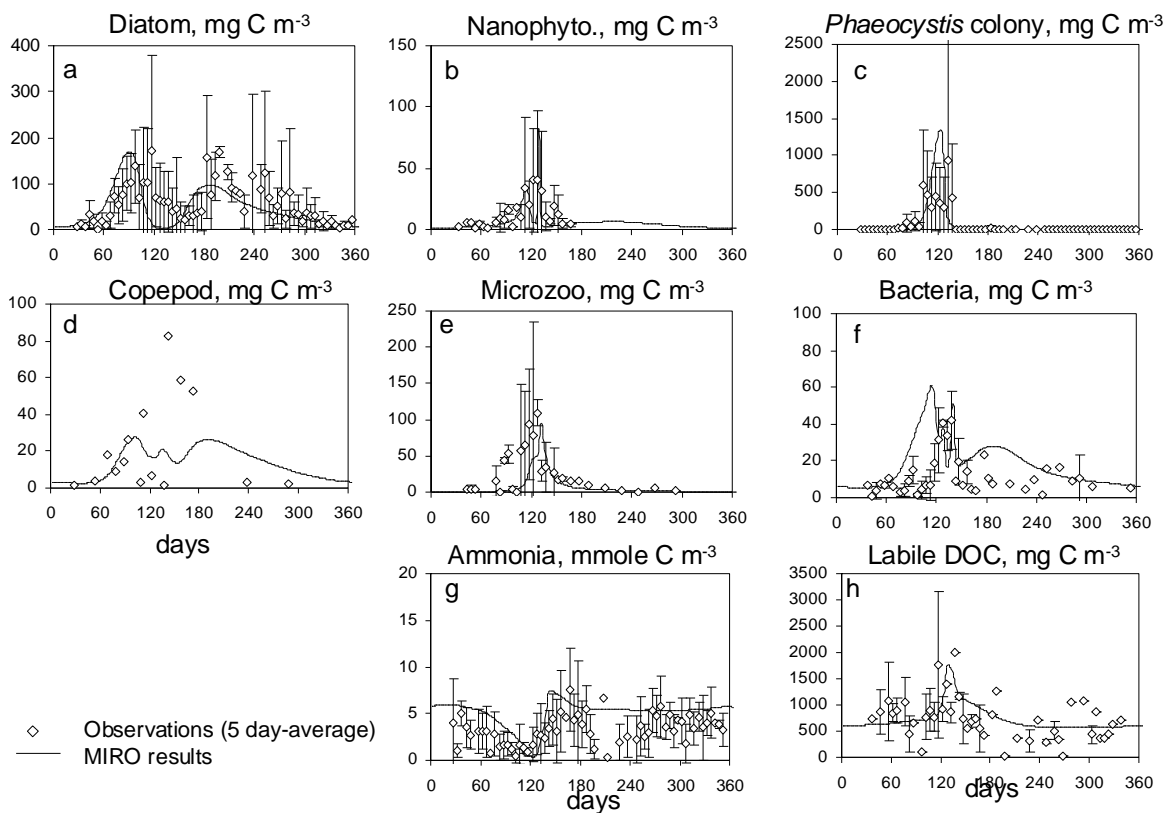


Figure 21: 0D-MIRO results (climatological run) and 1989-1999 observations at Station 330

4.2.1.4 Data assimilation: identification of important ecological parameters and errors estimation

The adjoint code of MIRO was developed to improve MIRO parameterisation and identify model pathways that are controlling the behaviour of the ecosystem as well as eventual missing pathways and errors due to unresolved physical processes (advection/diffusion) in 0D-MIRO. This constitutes a necessary step prior to using real data collected in BCZ. In order to systematically test the ability of the assimilation technique to recover model parameters, numerical experiments with simulated data (twin experiments) were first carried out. The twin experiments using model-generated observations can be considered as the best scenario where the data set is guaranteed to be consistent with the model, free of measurement error, and expressed in the same units as the model results. Practically OD-MIRO model was run for 1 year using initial conditions from the steady state solution in FCZ box. The model results were used to create the time series to be utilized during the assimilation procedure (Fig. 22).

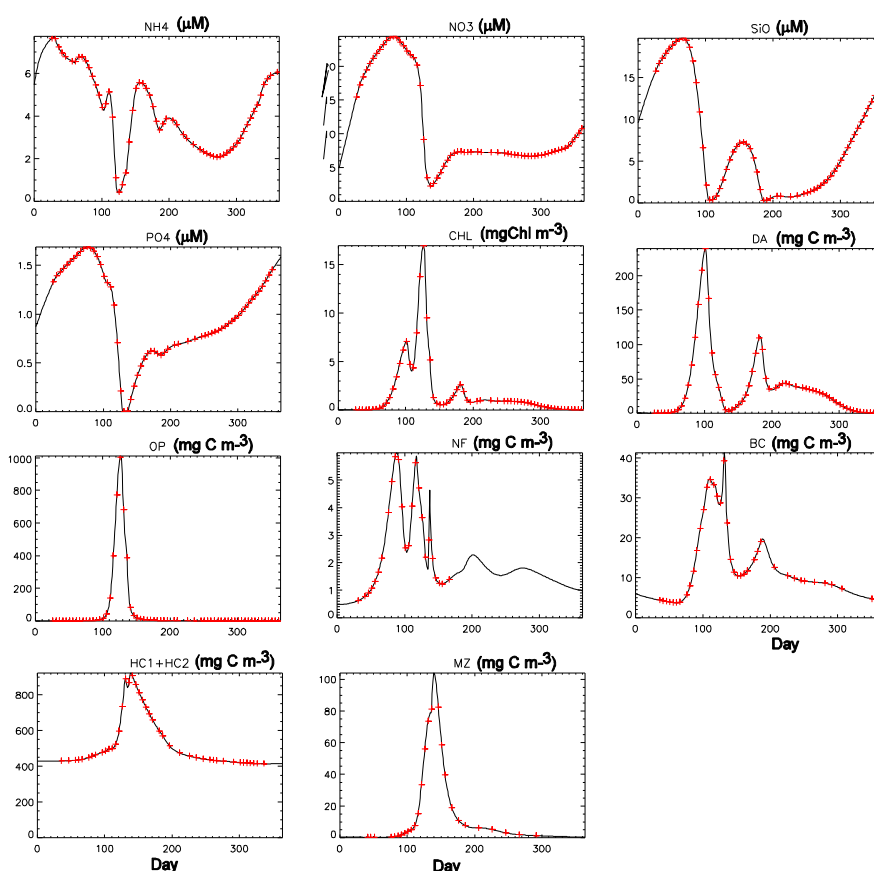


Figure 22. Model regenerated time series. The crosses indicate the sub-sampling equivalent to the sampling at station 330 between 1988 and 1999 (Rousseau, 2000)

Independence of MIRO parameters

Assimilation of hourly model-generated observations for the 32 state variables of MIRO was run with parameter first guesses taken as 70% of the “true” values. This experiment led to the recovery of all the parameters after about 1900 iterations, which indicates that all the parameters are independent. The cost function (Fig. 23a) decreased by 5 orders of magnitude during the first 200 iterations while it decreased by 8 orders of magnitude during the next 2000 iterations. The carbon ratios as well as some of the growth and grazing coefficients for phytoplankton and copepods were already recovered after 200 iterations (Fig. 24a). It is also interesting to note that four of the five coefficients related to the export to the benthos were also recovered. From the rapid decrease of the cost function during the first 200 iterations, we can conclude that these recovered parameters are controlling the behaviour of the model results. In addition, we found that the coefficient of vertical light attenuation as well as the photosynthetic capacity rate coefficients for diatom and *Phaeocystis* required over 1000 iterations to be recovered, which indicates that they are only weakly affecting the time evolution of the various concentrations. The meaning of these late recoveries will need to be further investigated. Indeed, the light limitation should be a strong controlling factor in the coastal area and the late recovery either indicates a high adaptation of phytoplankton to its low light environment or it is due to a non-realistic model parameterisation of the light limitation.

Relevance of the time-resolution of station 330 data set

These twin experiments were designed to assess the feasibility of parameter estimation when the observations at station 330 are used. We therefore created a time series of model-generated observations that are of the same type and sampling frequency as that of station 330 between 1988 and 2000 (Fig. 22). The twin experiments were also performed starting with 70% of the true values for the model parameters. The obtained convergence was much slower than when observations are available for all the state variables (Figs 23 and 24). The cost function decreased rapidly during the first 500 iterations, corresponding to the recovery of a parameter set similar to the one recovered with observations for all the 32 state variables. We then concluded that parameters describing growth and mortality of *Phaeocystis* colonies and diatoms as well as remineralisation (planktonic and benthic) are those controlling the ecosystem dynamics. After 15000 iterations, we found that the only parameters that are not recovered are the coefficient of vertical light attenuation, the photosynthetic capacity rate coefficients for diatoms and *Phaeocystis*, the carbon to chlorophyll coefficient, and the fraction of fecal pellets that goes to biodegradable dissolved and particulate organic matter (DOM and POM). This is consistent with the

findings from the experiment with observations for all the state variables, when the recovery of these parameters was the slowest (Fig.24). If we did not stop the recovery after 15000 iterations, we might have been able to recover all the parameters. However, the very high number of iterations indicates that some of the model pathways are not controlling the ecosystem. It might then be difficult to estimate the corresponding parameters when assimilating real observations with associated noise.

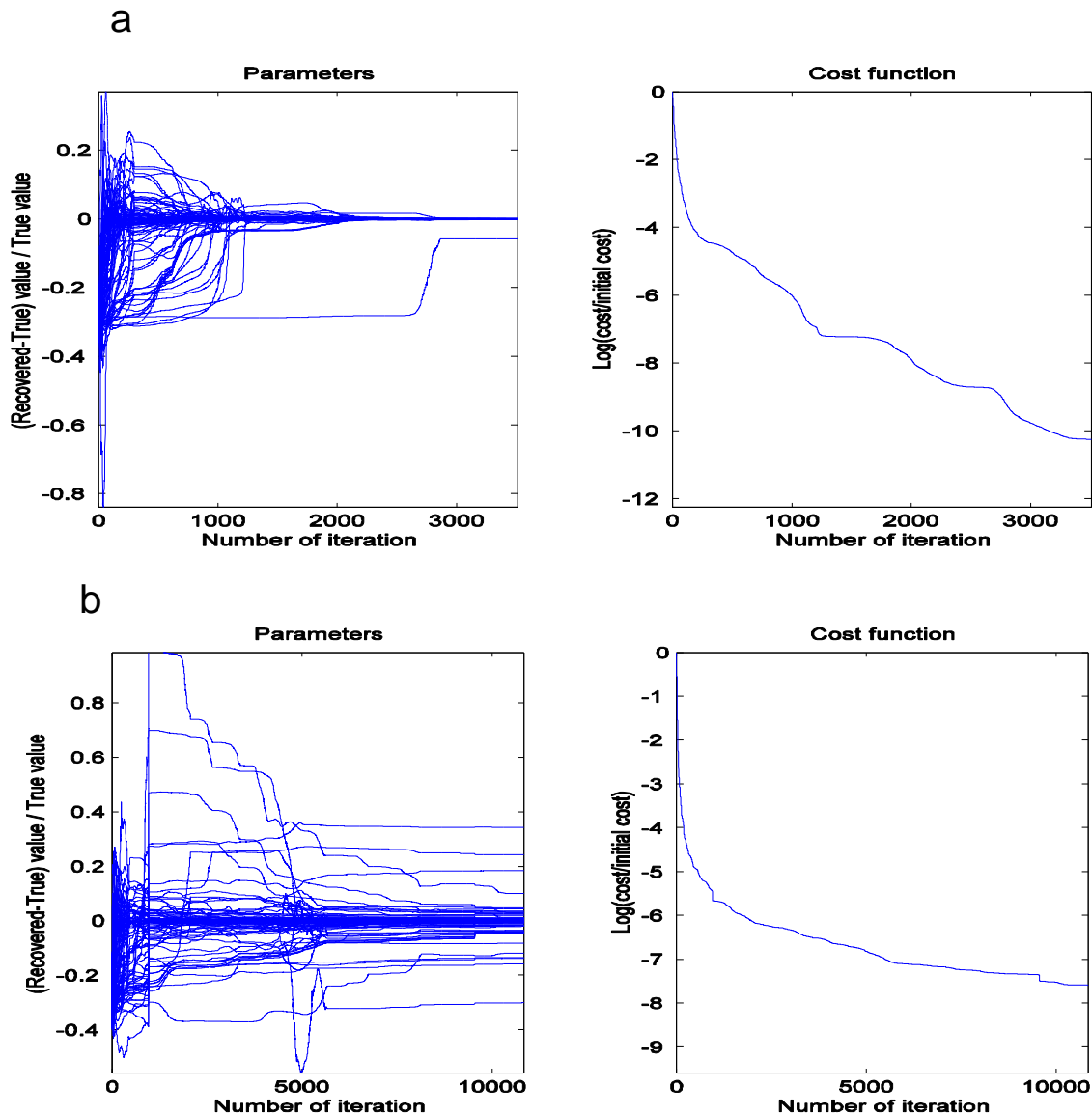


Figure 23: Recovery of the parameters when (a) hourly observations are available for the 32 state variables and (b) when observations corresponding to station 330 are available. The left panel represents the time evolution of the recovery and the right panel depicts the corresponding time evolution of the cost function.

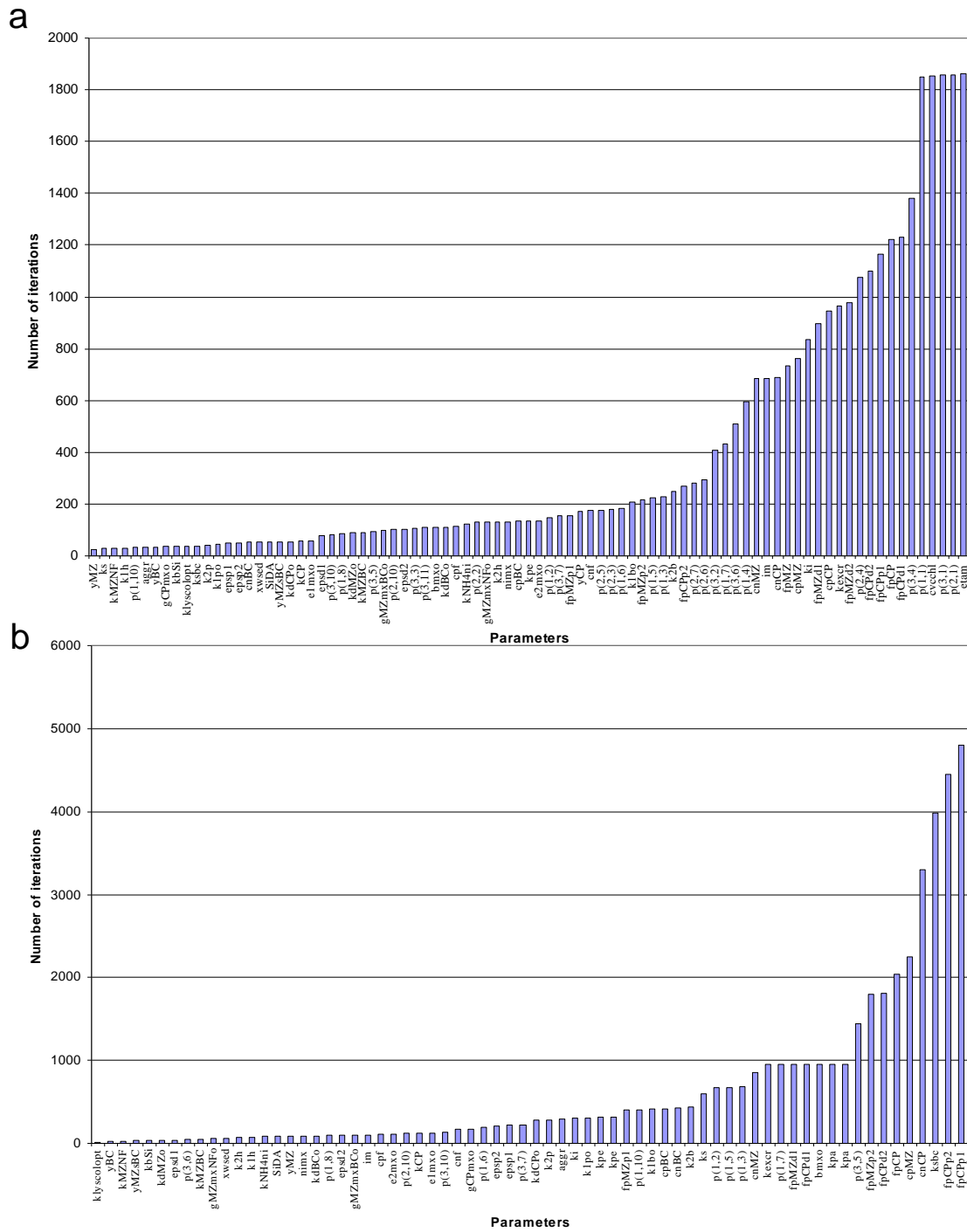


Figure 24: Recovery of the model parameters in function of the number of iteration when (a) hourly observations are available for the 32 state variables and (b) when observations corresponding to station 330 are available.

Estimation of model forcing due to the physics

Before assimilating the 330 data set it was felt necessary to run a third set of twin experiments for assessing the feasibility of parameter estimation when the observations are collected at one location in a strongly dynamical system such as the Southern Bight of the North Sea. Indeed, the Southern Bight of the North Sea is a strongly dynamical system where advection and diffusion are important. In addition, the river discharges can be important but not necessarily adequately measured. These two potential source/sink terms are not explicitly modelled in the 0D-MIRO. Several twin experiments (e.g. using observations obtained from a coupled 3D simulation) were then designed to show that it might be possible to estimate the source/sink terms due to advection/diffusion and river discharges. Fig. 25 shows an example of recovering the forcing due to “advection” and the river discharge. An example of the estimates of the forcing from the assimilation of a 3D run is shown in Fig. 26. Further work will explore the possibility of estimating the model parameters as well as the external forcing (advection/diffusion and river discharges) using twin experiments as well as assimilation of the station 330 observations. One has to realize that twin experiments are a prerequisite to understanding the results of real observation assimilation and therefore are necessary at each step of a given study.

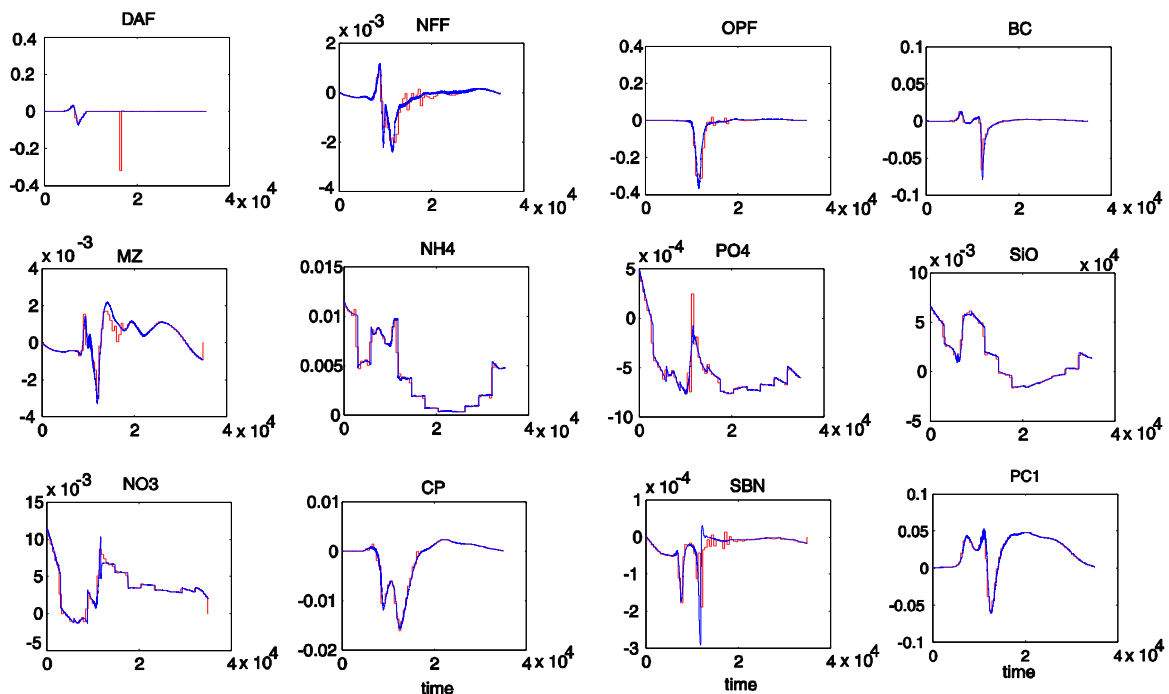


Figure 25: Recovery of the river and FCZ input. The blue lines represent the direct model sources and the red lines correspond to the estimated error from the absences of these sources. The time is expressed in number of 15min time steps, the y-axis has units of concentration per unit time.

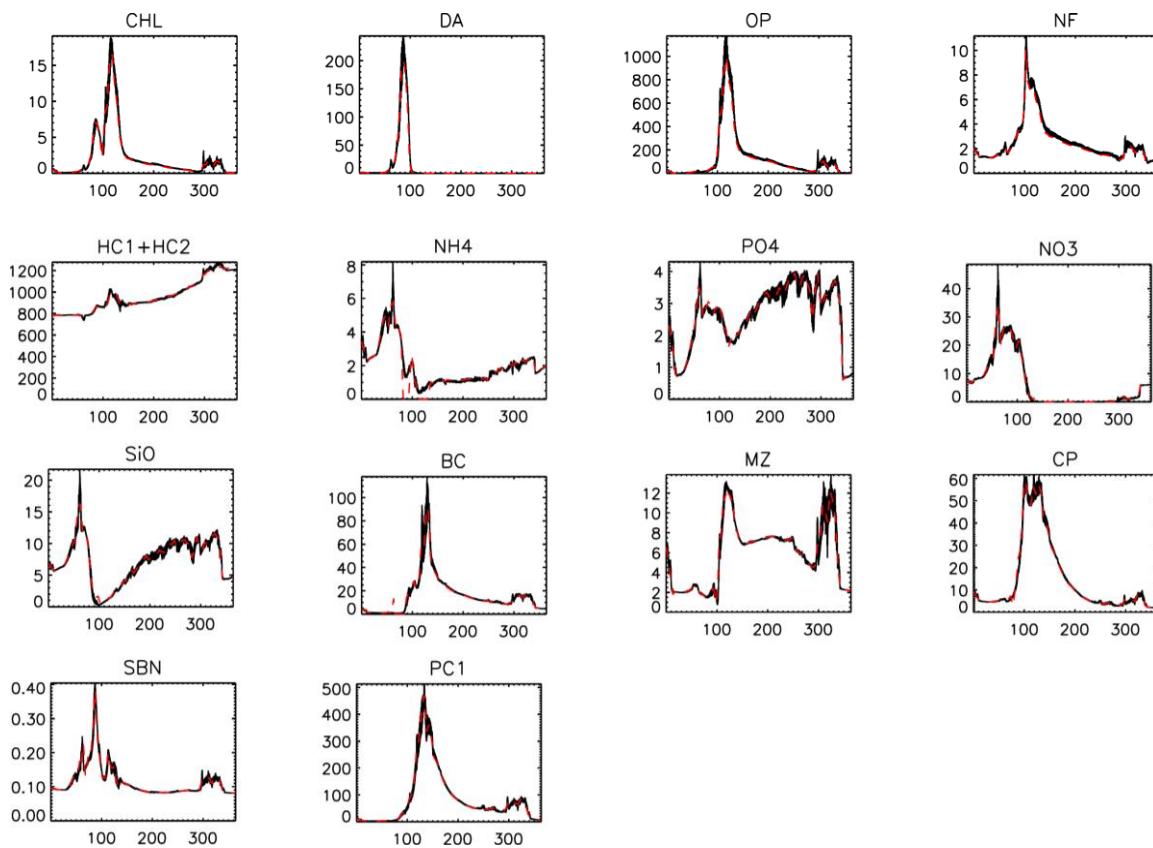


Figure 26: Recovery of the 3D time series obtained after 5000 iterations. The black lines are the 3D observations and the red lines are the 0D results when the physical forcing is estimated during the assimilation process.

4.2.2 Development and performance of the 3D MIRO&CO model

4.2.2.1 3D-COHSNS hydrodynamical modelling

The 3D-COHSNS hydrodynamic model was developed to trace the origin of freshwater in BCZ. The actual capability of 3D-COHSNS to simulate the salinity field can be appraised in Fig. 27 which compares the modelled surface salinity averaged over the year 1993 with available observations. Clearly 3D-COHSNS captures the band of lower salinity water along the Belgian and Dutch coasts identified by previous investigators (Lee 1980). The long-term average shown in Fig. 27 is only one aspect of the salinity distribution and does not reflect the strong dynamics in this region. The latter is driven by tidal currents and wind events (direction, speed and duration). Fig 27b shows the COHSNS predicted temporal distribution of salinity at three stations along an inshore-offshore gradient. In this figure sub-diurnal salinity variability can be attributed mainly to horizontal advection of salinity by tidal currents. On the other

hand, at time scales of a few days variability in salinity is caused by fluctuations in wind strength and direction.

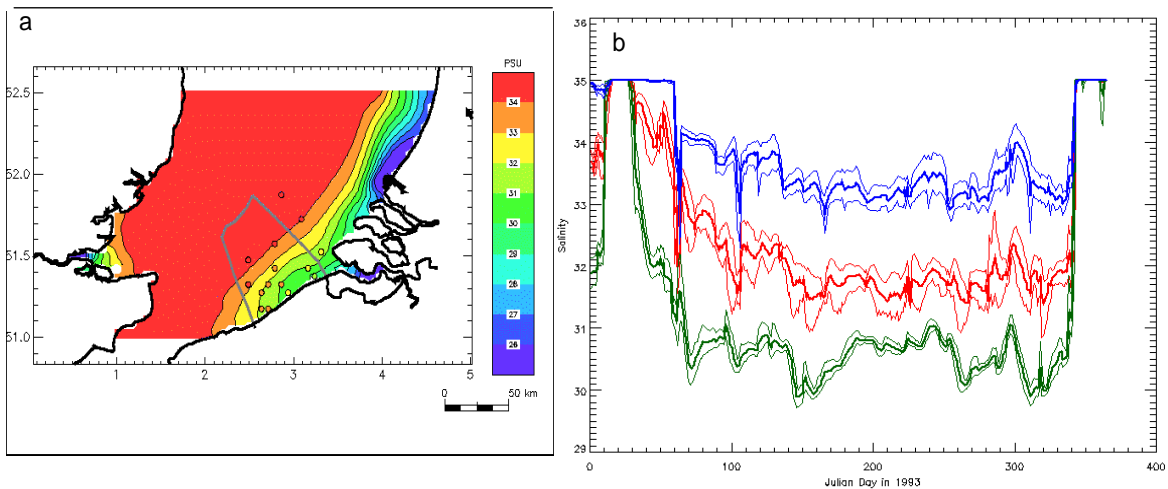


Figure 27: 3D-COHSNS simulation of surface salinity in 1993. (a) yearly average over the domain and (b) obtained at three stations: near-shore station 230 (green), the central station 330 (red) and the offshore station 435 (blue). The thick, solid lines represent the daily-averaged values, while daily minima and maxima are given by the surrounding thinner lines

Model tracers were further used to determine the origin of water masses in BCZ in terms of the model open sea and river estuary boundaries. Results (Fig. 28a) indicate that the salinity of Belgian waters is dominated by inflow of the Channel water mass which mixes with freshwater. The latter originates mainly from the Rhine/Meuse with a much smaller contribution from the Scheldt estuary (Fig. 28b). This result is further supported by simulations obtained when each river discharge is set to zero separately (Fig. 29). Clearly the freshwater which reduces salinity in the coastal strip of the BCZ with respect to offshore water originates primarily from the river Rhine and not, as supposed in previous studies, from the Scheldt estuary. The present numerical study thus suggests a major change of the conventionally accepted concept of the origin of water masses in this region. As illustrated in Fig. 30, this change considers not just the Northeastward residual current which would advect Rhine water away from the BCZ, but also the horizontal diffusion of freshwater induced by tidal advection which acts in both alongshore directions and over a considerable distance. In this simulation more than 1% of the water found at the French-Belgian coastal border originated from the Rhine and the salinity within the Scheldt estuary was significantly affected by freshwater from the Rhine intruding *via* the estuary mouth.

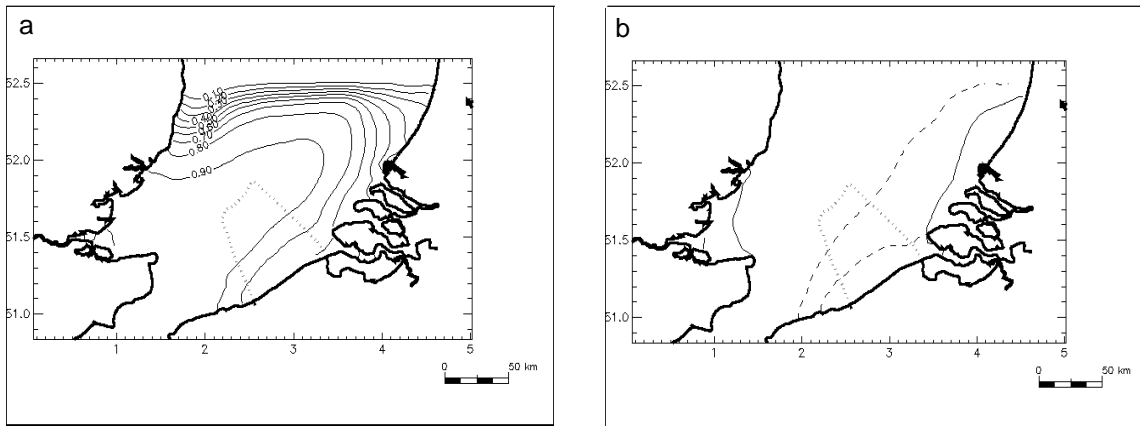


Figure 28. Map showing model results averaged over the duration of the 1993 simulation for (a:) tracer fractions of Channel water and (b) the 0.1 (=10%, solid line) and 0.01 (=1%, dashed line) tracer fractions for Rhine and Scheldt water.

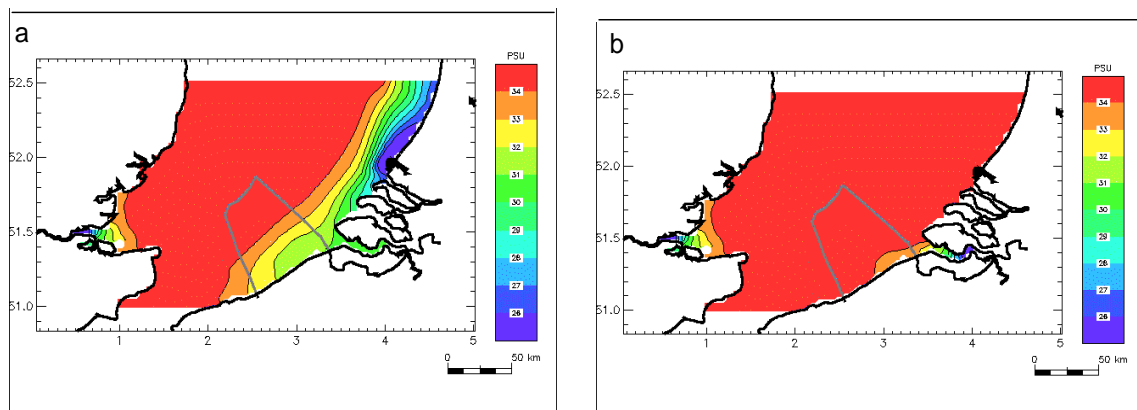


Figure 29. Surface salinity averaged over the duration of the 1993 simulation for model results with (a) Rhine discharge set to zero and (b) Scheldt discharge set to zero.

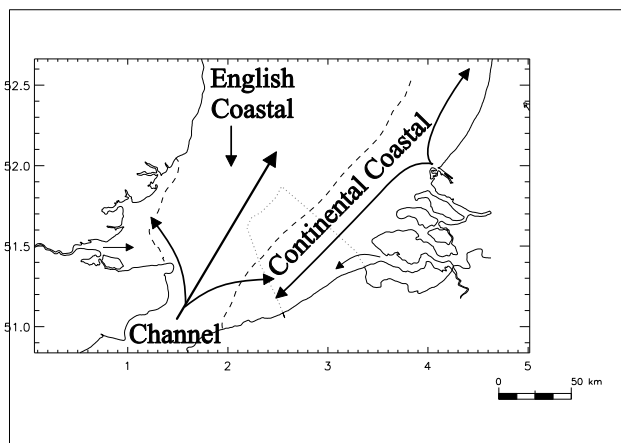


Figure 30. Conceptual model of water masses and dispersion of river water in the Southern Bight of the North Sea derived from the present study. Arrows denote dispersion paths, not residual currents.

4.2.2.2 3D MIRO&CO ecological modelling

The 3D-MIRO&CO ecological model was obtained by integrating the MIRO ecological model described in section 3.2.1. in the 3D-COHSNS hydrodynamical model. The obtained 3D-MIRO&CO calculates vertical and horizontal transport of the ecosystem and biogeochemical state variables. Model predictions thus produce information on the seasonal and geographical spreading of nutrients and phytoplankton blooms.

Seasonal trends

The model behaviour was first verified by comparing model output of the climatological run of 3D-MIRO&CO model at coordinates of station 330 with the corresponding 1989-1999 data set (Fig. 31) and predictions obtained with multi-box MIRO (Fig. 19-21). Main ecological trends (temporal succession of auto- and heterotrophic organisms and order of magnitude of biomass reached) and related nutrients are globally reproduced. However important discrepancies between predictions and observations are in the modelled PO_4 accumulation in fall and too low control of diatoms by copepod grazing. The latter feature was also in the multi-box MIRO predictions (Fig. 21). On the contrary the latter model reproduces quite well the observed PO_4 cycling (Fig.19) suggesting that sediments are not well constrained and parameterised in the 3D version of the ecological model. The general underestimate of MIRO&CO winter signature of nutrients correlates with overestimated salinity (not shown) suggesting that this discrepancy result of misrepresentation of hydrodynamic features including parameterisation of freshwater boundary conditions.

Spatial variability

Fig. 32 shows surface distribution in the whole geographical domain of nutrient and phytoplankton (Chl.a, diatom/*Phaeocystis* biomass) at different date of the spring bloom. One major feature is the strong coastal-offshore gradient due to river discharge of nutrients. Blooms start at the river mouths and spread offshore. 3D-MIRO&CO reproduces quite well the diatom-*Phaeocystis* succession, in particular the early spring spreading of diatoms which decline corresponds with dissolved silica depletion (Fig.32 b,e). *Phaeocystis* blooms after diatoms and deplete nitrates (Fig.32 a,f). These simulations give for the first time a picture of *Phaeocystis* spreading in the Southern Bight of the North Sea. A narrow offshore band except, it shows almost complete spring invasion of *Phaeocystis* blooms in the Belgian coastal zone (Fig.32f) which is currently observed (Rousseau et al., 2003).

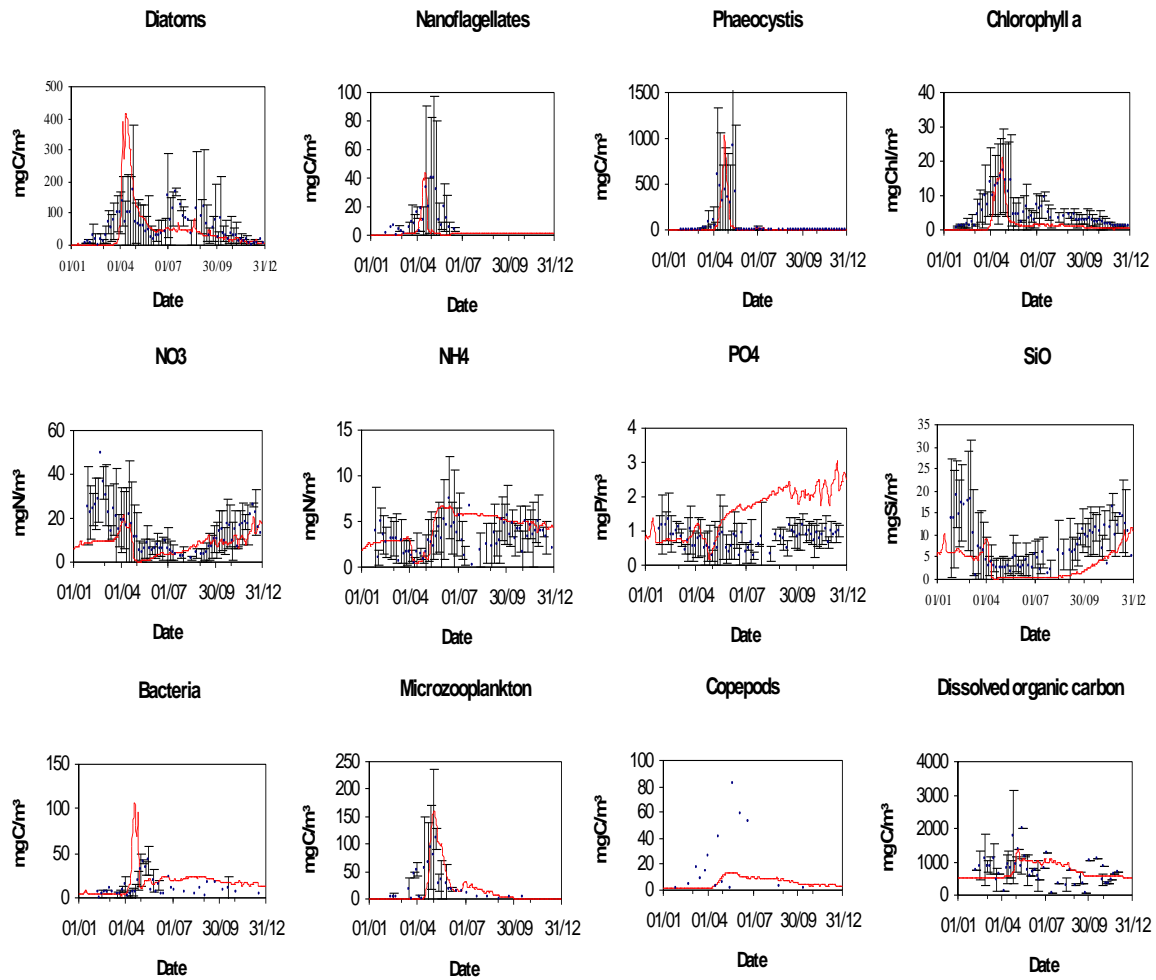


Figure 31: Results of the "climatological run" of MIRO&CO-3D model for station 330 (red line) compared to the available data for this station (5-day average over the period 1988-1999) (blue dots).

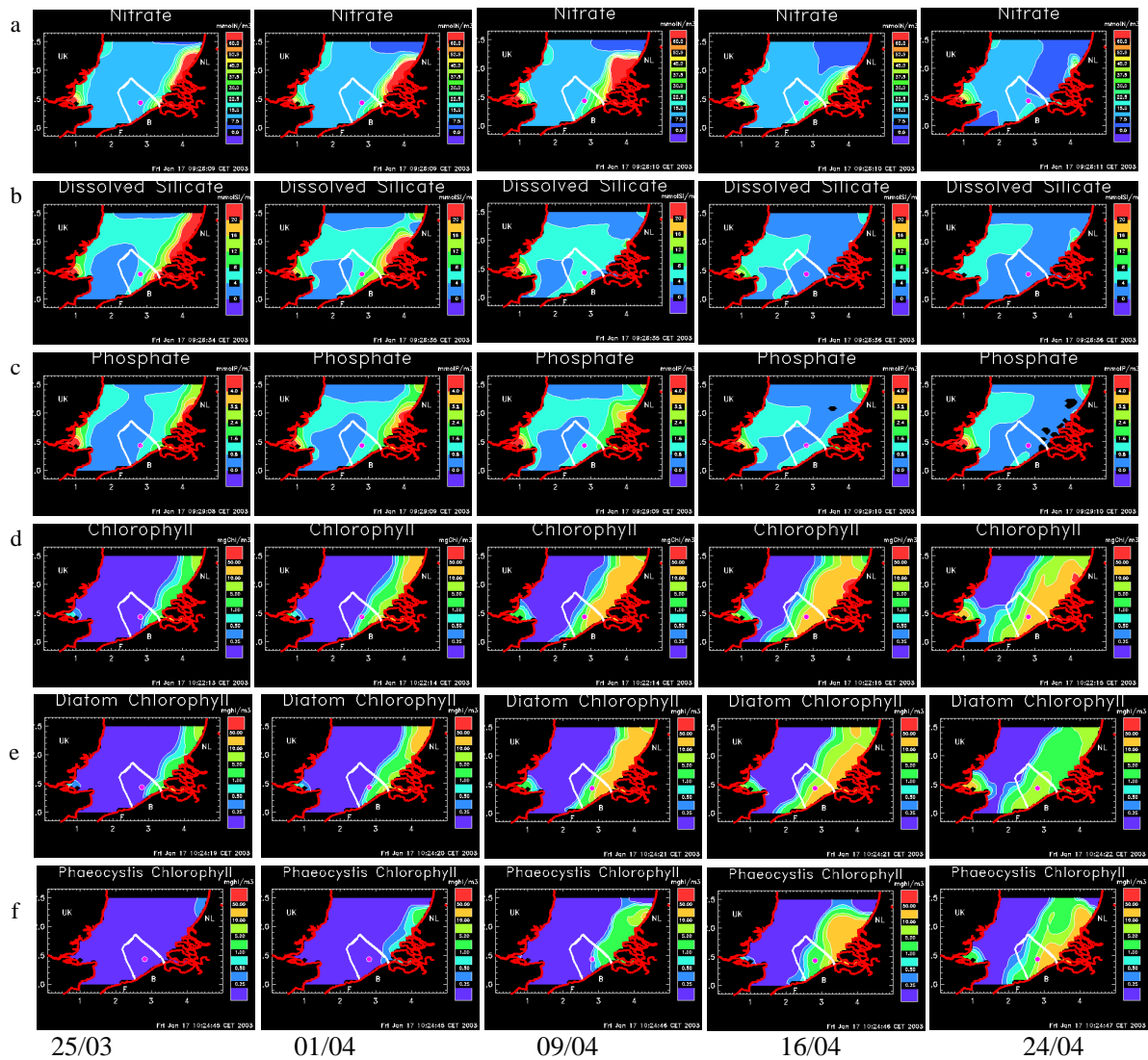


Figure 32: MIRO&CO-modelled geographical distribution of nutrients [nitrate (a), dissolved silica (b), phosphate (c)] and spreading of phytoplankton blooms [Chl.a (d), diatoms (e), Phaeocystis (f)] in spring at station 330 for the period 1989-1999 (climatology). Area delimited by the white frame corresponds to the BCZ.

4.2.3 Nutrient reduction scenarios

The Multi-box MIRO model was used to explore the impact of nutrient loads reduction on the magnitude of diatom and *Phaeocystis* colony blooms in the central BCZ (Station 330). For this preliminary study the model was run under 1989-1999 climatological forcing with varying (0 to 75%) reduction of nutrients discharged by on the river Scheldt. For these scenario's we explored the impact of either solely PO₄ or NO₃ or both N and P reduction on diatom and *Phaeocystis* blooms at station 330. Results (Fig. 33) show a different ecosystem response to the target nutrient. Shortly, PO₄ decreases slightly the magnitude of both diatom spring and summer blooms (Fig. 33a). Also the predicted height of the *Phaeocystis* colony bloom is lower than the reference run (Fig. 33d) suggesting that the magnitude of *Phaeocystis* colonies is sustained by regenerated forms of P derived from the mineralisation of spring diatom-derived matter. An opposite result is obtained with scenario's of NO₃ reduction predicting a significant decrease (30 to 60%) of *Phaeocystis* blooms (Fig. 33e) for the benefit of spring diatoms (Fig.33b). Interestingly enough NO₃ reduction leads to a slight decrease of the summer diatom bloom evidencing complex interactions between *Phaeocystis* colonies and these diatoms. Finally when both PO₄ or NO₃ are reduced, 0D MIRO predicts a reduction of all phytoplankton blooms (Fig. 33c,f) proportional to the extent of the nutrient reduction.

Finally we explored the impact of different nutrient reduction policies applied on the Scheldt and Rhine rivers with 3D-MIRO&CO forced with a 50% reduction of PO₄ and NO₃ applied to either the river Scheldt only or both the Scheldt and the Rhine. Results (Fig. 34) expressed in term of Chl a, an index of phytoplankton bloom, confirm the 30% bloom reduction obtained with 0D-MIRO. Moreover Fig. 34 shows that the magnitude of the spring phytoplankton bloom can be decreased by 50% when nutrient inputs by the Rhine are also reduced by 50%.

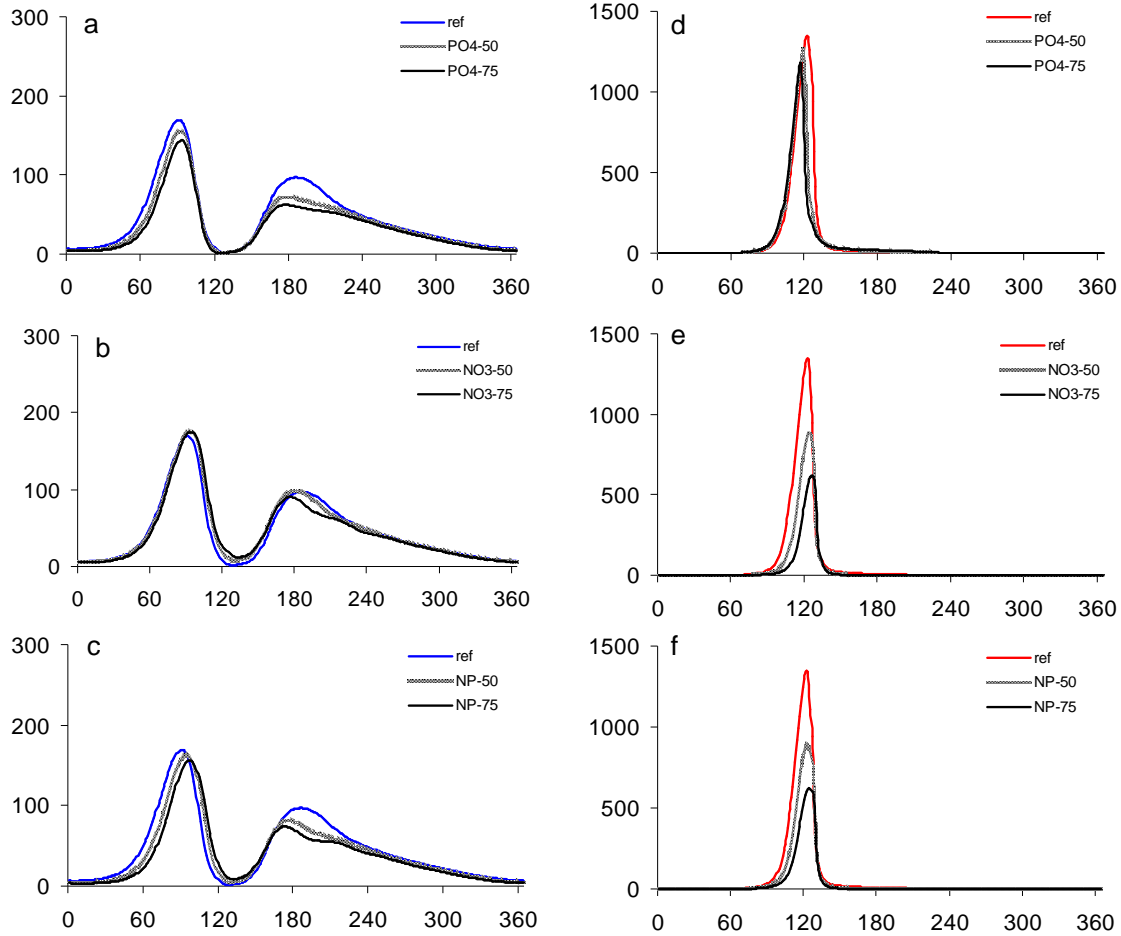


Figure 33: 0D-MIRO predictions of diatoms (left) and *Phaeocystis* (right) after reduction of riverine PO₄, NO₃ and NO₃+PO₄

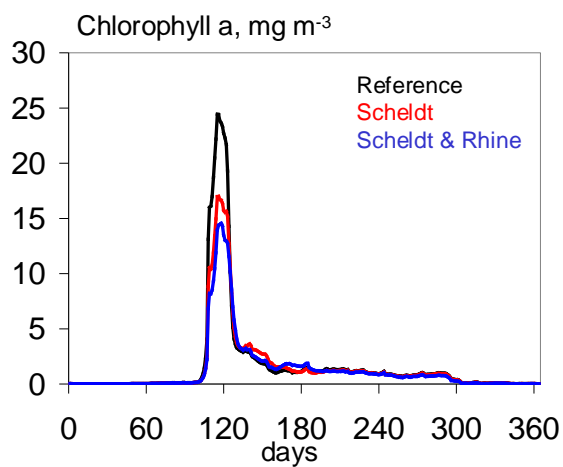


Figure 34: 3D-MIRO&CO predictions of phytoplankton after 50% reduction of nutrient (NO₃+PO₄) by the river Scheldt and Rhine

5 CONCLUSION

5.1 Eutrophication status of Belgian coastal waters

5.1.1 Nutrient enrichment and algal blooms

The Belgian Coastal Zone (BCZ) is part of the nutrient-enriched eastern Southern Bight of the North Sea invaded every spring by undesirable algal blooms reaching biomass higher than $30 \text{ mg Chl a m}^{-3}$. BCZ is a high dynamical system with waters resulting of the mixing between the in-flowing Atlantic waters and freshwater inputs from the IJzer, Scheldt and Rhine rivers. Numerical simulations with the 3D-COHSNS hydrodynamic model forced with *in situ* meteorological conditions clearly show that the geographical extend of the river plumes is driven by wind speed and direction under control of the North Atlantic Oscillation (NAO) index. Overall the nutrient enrichment in BCZ reflects the cumulative inputs of nutrients from atmospheric and direct sources, Scheldt, IJzer and Rhine rivers, local benthic remineralization and the in-flowing Atlantic waters themselves enriched by nutrient loads by the river Seine and Somme. The relative importance of these different sources in BCZ is not known yet and varies locally. Analysis of historical winter nutrient data from the Belgian monitoring network revealed a 50% reduction of PO_4 enrichment between 1972 and 1999 with no discernible change in dissolved inorganic nitrogen and silicate. Altogether these trends induced also significant qualitative (N:P:Si) changes in the nutrient coastal environment with however no observable impact on the magnitude of spring algal blooms regularly monitored at station 330 between 1988 and 2000. These blooms were recurrently characterised by the succession of three communities: the high-silicified early spring diatoms, the low-silica demanding *Chaetoceros spp* and *Guinardia spp*, and *Phaeocystis* colonies. The latter two communities were blooming together but their relative abundance displayed interannual variation which could not be related to the observed nutrient trends. Due to the dominance in spring of *Guinardia spp* in the BCZ in-fowing Atlantic waters further work will attempt to relate the *Phaeocystis-Guinardia* distribution to the hydrological signature of the water mass in the central BCZ.

5.1.2 Increased understanding of bottom-up controls of diatom/*Phaeocystis* colony successions

Beside nutrients, temperature and light are important “ bottom-up ” factors controlling bloom onset and species succession. Considerable progress based on observation and experimentation has been achieved in understanding their relative role in the control of phytoplankton successions in the BCZ. Evidence now exists that a light threshold of $12 \mu\text{mole m}^{-2} \text{ s}^{-1}$ in the water column is required for the onset of the

spring succession. This threshold is reached between mid-February and mid-March and relies on physical processes determining the load of suspended matter. This light level corresponds to the light required by early spring diatoms for an optimised cell division rate (Meyer et al., 2000). These early spring diatoms are also better competitive compared to *Phaeocystis* colonies at the low temperature of late-February early March (5-6°C; Rousseau, 2000). On the contrary, *Phaeocystis* colonies optimise their growth at higher temperature and light but are better flexible to light change (Meyer et al. 2000). It is therefore concluded that, in the absence of any other limitation, *Phaeocystis* colonies are able to outcompete early spring diatoms at the higher light intensity of April. On the other hand, difference in temperature adaptation could not be evidenced for *Phaeocystis* and *Guinardia spp.* which are blooming together. Seasonal changes of nutrients suggest that the magnitude of the early spring diatom bloom is controlled by the availability of both PO_4 and $\text{Si}(\text{OH})_4$ and that the silicification level is related to ambient silicic acid (Rousseau et al., 2002). This observation, also supported by 0D-MIRO model runs, suggests that “excess new nitrates” (i.e. left over after early spring diatom growth) but regenerated PO_4 and Si (for diatoms only) sustain the growth of *Phaeocystis* and *Guinardia*. For the first time, PO_4 limitation was demonstrated in the BCZ via the detection of alkaline phosphatase activity in spring. One major result is that this enzymatic activity is associated to mainly large particles including phytoplankton cells and their attached bacteria. The highly significant correlation between alkaline phosphatase activity and *Phaeocystis* suggests that the colonies play a major role in PO_4 regeneration and are cleaving organically-bound phosphorus for their own utilisation, hence competing with bacteria for phosphate uptake during this period of low ambient phosphate. Further investigations making use of specific probes for locating alkaline phosphatase on cell membrane are required for stating on the mixotrophy ability of *Phaeocystis*.

5.1.3 Food-web structure and trophic efficiency

Specific grazing experiments conducted during AMORE (Gasparini et al., 2000) clearly demonstrated that *Phaeocystis* colonies are not grazed by indigenous zooplankton (*Temora longicornis*) but the reason was not identified. Process-level studies conducted in spring 1998 allowed calculating the budget of carbon transfer through the planktonic network (Rousseau et al., 2000). This calculation indicates that most of *Phaeocystis* production escapes direct grazing and flows through the microbial network where *Phaeocystis* cells are grazed by microzooplankton and *Phaeocystis*-derived DOC is rapidly recycled. This suggests that *Phaeocystis*-derived organic matter is biodegradable and that insignificant carbon is transferred to

mesozooplankton and exported to the sediment. Fieldwork conducted in spring 1999 and 2000 concluded indeed that most of organic matter synthesised during the spring bloom is biodegradable *per se* (Déliat et al., 2003). The very low bacterial growth yield of 0.1 (Déliat et al., 2003) indicates that most organic carbon taken up is mineralised rather than building biomass. This result agrees very well with the low trophic efficiency of the microbial food web estimated by Rousseau et al. (2000), based on independent budget calculations. Also in agreement with budget calculation, the potential sinking rates of *Phaeocystis* colonies were negative for colony sizes > 250 µm. Based on this carbon budget, it was further hypothesized that adult copepods would be in food shortage during *Phaeocystis* blooms which could impact negatively not only on the next generation of copepods but also on fish recruitment by starvation of fish larvae. This hypothesis is however challenged by additional field data on egg production by copepods suggesting alternate sources of good quality food for copepods. Yet the trophic pathways are even more complex due to the presence between April and June of a huge mass of gelatinous zooplankton. Main species are the Appendicularian *Oikopleura dioica* occurring at high density (~ 4500 ind m⁻³) before and after *Phaeocystis*, the ctenophores *Pleurobrachia* at the decline of *Phaeocystis* and the dinoflagellate *Noctiluca scintillans* forming often red tides in June (Schoemann et al., 1998). Little is known about the trophic status of these gelatinous organisms due to their extreme fragility and the difficulty of sampling undamaged organisms. Current knowledge reports these gelatinous as opportunistic and voracious and it might be that *O. dioica* and *N. scintillans* are those who benefit from *Phaeocystis* matter and the associated bacteria. The presence of *Pleurobrachia* is more worrying as ctenophores are generally reported as carnivorous, feeding on fish larvae and competing with them for copepods. Gelatinous zooplankton is on the other hand considered as trophic dead-end and large amounts of NH₄ and PO₄ are released as catabolic products or after their death. In agreement, huge accumulations of NH₄ and to a lesser extent PO₄ have been recorded in the BCZ at *N. scintillans* bloom decline. However some other observations reporting *O. dioica* as preferred food of flatfish larvae suggest that carbon and nutrient recycling might not be the unique role of gelatinous in the BCZ. Clearly additional ecological studies involving copepods, gelatinous zooplankton, bacteria and fish larvae have to be conducted at the time of *Phaeocystis* blooms and decline to better assess the impact of *Phaeocystis* blooms on higher trophic levels and the resulting effect on nutrient retention in BCZ.

5.2 Assessment and mitigation tools

5.2.1 Prediction capability

Due to the complexity of bottom-up and top-down controls of marine food webs and hydrodynamic features in BCZ, the link between human activity and the response of the coastal ecosystem cannot be understood by simple correlation's between events. Coupled physical-biological models which are based on physical, chemical and biological principles and describe ecosystem carbon and nutrient cycles as a function of environmental pressure are ideal tools to handle this complexity. When properly validated, these models can be used to explore the ecosystem response in term of algal blooms magnitude and extent to changes in land-based nutrients and short-term climate. A 3D-ecological model (3D-MIRO&CO) of high spatial and trophic resolution to resolve the changing nutrients loads, the complex biology and hydrodynamics and the tight coupling between the benthic and pelagic realm that characterizes BCZ has been successfully implemented. The model results of the online coupling of the 3D-COHSNS hydrodynamic model and an upgraded version of the ecological model MIRO based on process-level studies and making use of new data assimilation technics for improving model parameterisation. For this reason the model is in continuous evolution relying on new knowledge gained on mechanisms behind coastal eutrophication and progress achieved by data assimilation. Hence the methodology implemented by AMORE involves and combines in an interactive way 0D and 3D ecological modelling and data assimilation technics.

The 3D-MIRO&CO model developed by AMORE was run to simulate the annual cycle of inorganic and organic nutrients, phytoplankton (diatoms & *Phaeocystis*), bacteria and zooplankton (microzooplankton & copepods) in the Southern Bight of the North Sea for the period 1995-1999. These model runs gave a first view of spatial variability within the domain. The results demonstrated a number of observed processes such as the diatom-*Phaeocystis* succession and the related depletion of silicates and nitrates; the seasonal evolution and magnitude of bacteria, micro- and meso-zooplankton. Less simulated are the seasonal evolution of copepods and PO₄, the transient accumulation of ammonium in June and the summer and fall diatoms. This was attributed to unappropriated parameterization of mesozooplankton feeding and the low description of processes involved in phosphorus benthic diagenesis. Interestingly enough the spreading of the Rhine fresh waters evidenced with 3D-COHSNS tracers studies (Ruddick et al., 2003) was not shown to bring significant inorganic nutrients in the BCZ due to their consumption outside the simulated 3D-MIRO&CO domain.

5.2.2 Mitigation

0D-MIRO model scenarios conducted with changing N and P delivery to BCZ by the river Scheldt suggest that the highest reduction of *Phaeocystis* colony blooms can be reached by reducing Scheldt NO₃ delivery by 75%. This reduction might however be too strong as it also decreases the magnitude of the summer diatom bloom which sustains the growth of mesozooplankton. Interestingly enough PO₄ reduction has little impact on the *Phaeocystis* bloom and the reduction of N and P decreased the magnitude of both diatom and *Phaeocystis* blooms. Additional scenarios conducted with 3D-MIRO&CO and exploring the additional impact of the reduction of Rhine nutrients indicate a little effect compared to that obtained by reducing the only Scheldt river inputs. We then conclude that, according to our present knowledge, NO₃ discharged by the Scheldt river should be the target nutrient to be reduced for obtaining a significant decrease of *Phaeocystis* colony blooms in the BCZ.

6 ACKNOWLEDGEMENT

The present work is a contribution of the AMORE (Advanced MOdeling and Research on Eutrophication) project of the Belgian Programme “Scientific Support Plan for a Sustainable Development Policy-Sustainable Management of the North Sea” funded by the Belgian Science Policy under contract # MN/DD/20-21-22. The work also benefits from results gained by the teams in the scope of projects funded by several Belgian North Sea and EU-Environment Programmes since 1988. We are indebted to the successive captains and crew of R.V. Belgica and our fellow colleagues from Belgian marine institutions for helping in the weekly sampling of Station 330.

7 REFERENCES

- Becquevort, S. 1987. Etude de la predation des bactéries par les microprotozoaires hétérotrophes en milieux aquatiques. Master thesis. Université Libre de Bruxelles.
- Becquevort, S., Rousseau, V. and Lancelot, C., 1998. Major and comparable roles for free-living and attached bacteria in the degradation of *Phaeocystis*-derived organic matter in the Belgian coastal waters of the North Sea. *Aquat. Microb. Ecol.*, 14: 39-48.
- Bienfang, P.K. 1981. SETCOL A technologically simple and reliable method for measuring phytoplankton sinking rates. *Canadian Journal of Fisheries and Aquatic Sciences*, 38, 1289-1294.

- Billen, G. and P. Servais, 1989. Modélisation des processus de dégradation bactérienne de la matière organique en milieu aquatique. In : Micro-organismes dans les écosystèmes océaniques. Bianchi et coll. Masson. p. 219-245.
- Billen, G., Dessery, S., Lancelot, C. & Meybeck, M., 1989. Seasonal and interannual variations of nitrogen diagenesis in the sediments of a recently impounded basin, Biogeochemistry, 8 : 73-100.
- Block, J. C., Mathieu, L., Servais, P., Fontvieille, D. and Werner, P., 1992. Indigenous bacterial inocula for measuring the biodegradable dissolved organic carbon (BDOC) in waters. Wat. Res., 26: 481-486.
- Brzezinski MA. 1985. The Si:C:N ratio of marine diatoms: interspecific variability and the effect of some environmental variables. J. Phycol. 21: 347-357.
- Conley, D.J, Kilham S.S and Theriot, E.1989. Differences in silica content between marine and freshwater diatoms. Limnol Oceanogr 34: 205-213
- Creutzberg, F. and Postma,H. 1979. An experimental approach to the distribution of mud in the southern North Sea. Neth. J. Sea Res. 13, 99-116.
- Daro, M.-H. 1985. Field study of the diel, selective and efficiency feeding of the marine copepod *Temora longicornus* in the Southern Bight of the North Sea. In: Proceedings Progress in Belgian Oceanographic research, Brussels, March 1985, pp 250-259.
- Daro, M.-H. and van Gijsegem, B. 1984. Ecological factors affecting weight, feeding and production of five dominant copepods in the Southern Bight of the North Sea. Rapp. P.-V. rein. Cons. Int. Explor. Mer, 183, 226-233.
- Del Amo, Y., Le Pape, O., Tréguer, P., Quéguiner, B., Ménesguen, A. and Aminot, A 1997a. Impact of high-nitrate freshwater inputs on macrotidal ecosystems. I. Seasonal evolution of nutrient limitation for the diatom-dominated phytoplankton of the Bay of Brest (France). Mar. Ecol. Progr. Ser. 161: 213-224
- Del Amo, Y., Quéguiner, B., Tréguer, P., Breton, H. and Lampert, L. 1997b. Impact of high-nitrate freshwater inputs on macrotidal ecosystems. II. Specific role of the silicic acid pump in the year-round dominance of diatoms in the bay of Brest (France). Mar. Ecol. Progr. Ser. 161: 225-237
- de Vries H., Breton M., Mulder T.d., Krestenitis Y., Ozer J., et al, 1995. A comparison of 2D storm surge models applied to three shallow European seas. Environmental Software 10, 23-42.
- Deleersnijder E., Wolanski E., Norro A., 1989. Numerical simulation of the three-dimensional tidal circulation in an island's wake. In: GM Carlomango, CA Brebbia (Eds.), Computers and experiments in fluid flow, Springer-Verlag, pp. 355-381.

- Edler, L. 1979. Recommendations for marine biological studies in the Baltic Sea. *Phytoplankton and Chlorophyll*. Baltic Marine Biologists Publ 5 : 1-38
- Gasparini, S., Daro, M.-H., Antajan, E., Tackx, M., Rousseau, V., Parent, J.-Y., Lancelot, C., 2000. Mesozooplankton grazing during the *Phaeocystis globosa* bloom in the Southern Bight of the North Sea. *Neth. J. Sea Res.* 43, 345-356.
- Gilbert J.-Ch., and C. Lemaréchal, 1989. Some numerical experiments with variable-storage quasi-Newton algorithms. *Mathematical Programming*, 45, 407-435.
- Grall, J-R .1972. Développement printanier de la diatomée *Rhizosolenia delicatula* près de Roscoff. *Mar Biol* 16 : 41-48.
- Grasshoff, K., Ehrhardt, M. and Kremling, K. 1983. *Methods of seawater analysis*. Verlag-Chemie Weinheim, New-York.
- Hamm, C., Simson, D., Merkel, R. and Smetacek, V. 1999. Colonies of *Phaeocystis globosa* are protected by a thin but tough skin. *Mar. Ecol. Progr. Ser.*, 187:101-111.
- Hansen, B., Verity, P., Falkenhaus, T., Tande, K. S., and Norrbin, F. 1994. "On the trophic fate of *Phaeocystis pouchetii* (Harriot). V. Trophic relationships between *Phaeocystis* and zooplankton: an assessment of methods and size dependence." *Journal of Plankton Research*, 16(5), 487-511.
- Hill, M.O. 1979. TWINSPLAN: A computer program for arranging multivariate data in an ordered two-way table for classification of the individuals and attributes. Section of Ecology and Systematics, Cornell University, New-York.
- Hurtt, G.C. and R.A. Armstrong. 1999. A pelagic ecosystem model calibrated with BATS data and OWSI data. *Deep-Sea Res. II*, 46, 27-61.
- Lancelot, C. and Billen, G., 1985. Carbon-Nitrogen relationship in nutrient metabolism of coastal marine ecosystem. *Advances in Aquatic Microbiology*. H.W. Jannash & P.J. Leeb Williams, Academic Press London, 3 : 263-321.
- Lancelot, C. and Mathot, S., 1985. Biochemical fractionation of primary production by phytoplankton in Belgian coastal waters during short- and long-term incubations with ^{14}C -bicarbonate. I. Mixed diatom population. *Mar. Biol.*, 86(3) : 219-226.
- Lancelot, C., Billen, G., Sournia, A., Weisse, T., Colijn, F., Veldhuis, M., Davies, A. & Wassman, P., 1987. *Phaeocystis* blooms and nutrient enrichment in the continental coastal zones of the North Sea. *Ambio*, 16 : 38-46.
- Lancelot, C. 1995. The mucilage phenomenon in the continental coastal waters of the North Sea. *The Science of the Total Environment* 165: 83-102.
- Lancelot et al., 1987
- Lancelot, C., Veth, C. and Mathot, S., 1991. Modelling ice edge phytoplankton bloom in the Scotia Weddell Sea sector of the Southern Ocean during spring 1988. *Journ.Mar.Syst.*, 2 : 333-346.

- Lancelot, C., Rousseau, V., Billen, G. and Eeckhout, D.V., 1997. Coastal eutrophication of the Southern Bight of the North Sea: Assessment and modelling. In: E. Ozsoy and A. Mikaelyan (Editors), Sensitivity to change: Black Sea, Baltic Sea and North Sea. NATO-ASI. Kluwer, Netherlands, pp. 437-454.
- Lancelot, C., Keller, M.D., Rousseau, V., Smith, Jr WO. And Mathot, S. 1998. Autoecology of the Marine Haptophyte *Phaeocystis* sp. In: Anderson DM, Cembella AD, Hallegraeff GM (eds) Physiological Ecology of Harmful Algal Blooms. NATO ASI Series. Springer-Verlag Berlin, p 209-224
- Lancelot, C., Spitz, Y., Gypens, N., Ruddick, K., Becquevort, S., Rousseau, V. and G. Billen, G. Modelling diatom-*Phaeocystis* blooms and nutrient cycles in the eutrophicated Belgian coastal waters (Southern Bight of the North Sea). I the 1988-1999 period.
- Lawson, L. M., Y. H. Spitz, E. E. Hofmann, and R. B. Long, 1995. A data assimilation technique applied to a predator-prey model. *Bulletin of Math. Biology*, 57, 593-617.
- Lawson, L. M., E. E. Hofmann, and Y. H. Spitz, 1996. Time series sampling and data assimilation in a simple marine ecosystem model. *Deep-Sea Res. II*, 43, 625-651.
- Lee A.J., 1980. North Sea: Physical Oceanography. In: MBCaKSM F.T. Banner (Eds.), *The North-West European Shelf Sea: The seabed and the sea in motion II. Physical and Chemical Oceanography, and Physical resources*, Elsevier, Amsterdam, pp. 467-493.
- Lorenzen, G.J. 1967. Determination of chlorophyll and phaeopigments: spectrophotometric equations. *Limnol. Oceanogr.*, 12: 343-346.
- Luyten P.J., Jones J.E., Proctor R., Tabor A., Tett P., Wild-Allen K., 1999. COHERENS documentation: A coupled hydrodynamical-ecological model for regional and shelf seas: user documentation, MUMM, Brussels.
- Marshall, J., Kushnir, Y., Battisti, D., Chang, P., Hurrell, J., McCartney, M. and M. Visbeck. 1997. A white paper on Atlantic climate variability. <http://geoid.mit.edu/accp/avehtml.html>
- Mathot, S., Lancelot, C. & Dandois, J.M., 1992. Gross and net primary production in the Scotia Weddell sector of the Southern Ocean during spring 1988. *Polar Biol.*, 12 : 321-332.
- Myklestad, S. M., Skånøy, E. and Hestmann, S., 1997. A sensitive and rapid method for analysis of dissolved mono- and polysaccharides in seawater. *Mar. Chem.*, 56: 279-286.
- Nelson, D. and Smith, W.O. 1986. Phytoplankton bloom dynamics of the western Ross Sea ice edge -II. Mesoscale cycling of nitrogen and silicon. *Deep-Sea Res* 33: 1389-1412

- Porter, K. G. and Feig, Y. S., 1980. The use of DAPI for identifying and counting aquatic microflora. *Limn. Oceanogr.*, 25: 943-948.
- Radach, G., Pätsch, J., Gekeler, J. and Herbig, K., 1995. Annual cycles of nutrients and chlorophyll in the North Sea. *Ozeanographie berichte 20*, Zentrum für Meeres- und Klimaforschung.
- Ragueneau, O. and Tréguer, P. 1994. Determination of biogenic silica in coastal waters: applicability and limits of the alkaline digestion method. *Mar. Chem.*, 45: 43-51.
- Ragueneau, O., De Blas Varela, E., Tréguer, P., Quéguiner, B. and Del Amo, Y. 1994. Phytoplankton dynamics in relation to the biogeochemical cycle of silicon in a coastal ecosystem of Western Europe. *Mar Ecol Progr Ser* 106:157-172
- Redfield, A.C., B.A. Ketchum and F.A. Richards. 1963. The influence of organisms on the composition of sea-water, p 26-77. In: *The sea*. M.N. Hill (Ed). Wiley.
- Rijkswaterstaat, T.W.D., 1992. Guidance document for the NSTF modelling workshop 6-8th May, 1992, Hague
- van Rijssel, M., Hamm, C. and W. Gieskes. 1997. *Phaeocystis globosa* (Prymnesiophyceae) colonies: hollow structures built with small amounts of polysaccharides. *Eur. J. Phycol.*, 32: 185-197.
- Rousseau, V., Vaultot, D., Casotti, R., Cariou, V., Lenz, J., Gunkel, J. & Bauman, M. 1994 The life-cycle of *Phaeocystis* (Prymnesiophyceae) : evidence and hypotheses, *Journ.Mar.Syst.* 5(1): 23-39.
- Rousseau, V., Mathot, S. and C. Lancelot. 1990. Calculating carbon biomass of *Phaeocystis* sp. from microscopic observations. *Mar. Biol.* 107: 305-314.
- Rousseau, V. 2000. Dynamics of *Phaeocystis* and diatom blooms in the eutrophicated coastal waters of the Southern Bight of the North Sea. PhD Thesis, Université Libre de Bruxelles.
- Rousseau, V., Leynaert, A., Daoud, N. and C. Lancelot. 2002. Diatom succession, silicification and silicic acid availability in Belgian coastal waters (Southern Bight of the North Sea). *Mar. Ecol. Progr. Ser.* 236: 61-73
- Rousseau, V., S. Becquevort, J.Y. Parent, S. Gasparini, M.-H. Daro, M. Tackx & C. Lancelot. 2000. Trophic efficiency of the planktonic food web in a coastal ecosystem dominated by *Phaeocystis* colonies. *J. Sea Res.* 43:357-372.
- Rousseau, V., Breton, E., de Wachter, B., Beji, A., Deconinck, M., Huijgh, J., Bolsens, T., Leroy, D., Jans, S., and Lancelot C. 2003. Identification of Belgian maritime zones affected by Eutrophication (IZEUT). Final Report. OSTC publications.

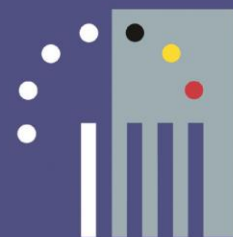
- Ruddick K.G., 1995. Modelling of coastal processes influenced by the freshwater discharge of the Rhine. PhD thesis. Université de Liège. 247 pp.
- Ruddick, K., Ozer, J. and Lancelot, C. 2003. Modelling the impact of the Scheldt and Rhine/Meuse plumes on the salinity distribution in Belgian waters (Southern North Sea). Submitted to J. Sea Res.
- Schoemann, V., de Baar, H. J. W., de Jong, J. T. M., and Lancelot, C. 1998. Effects of phytoplankton blooms on the cycling of manganese and iron in coastal waters. *Limnol. and Oceanogr.*, 43(7), 1427-1441.
- Servais, P. 1990. Estimation de la production bactérienne en milieu marin par mesure du taux de synthèse protéique. *Oceanol. Acta*, 13 : 229-235.
- Servais, P., Billen, G. and Hascoët, M.-C., 1987. Determination of the biodegradable fraction of dissolved organic matter in waters. *Wat. Res.*, 21: 445-450.
- Sournia, A., Birrien, J-L., Douvillé J-L., Klein B. and Viollier, M .1987. A daily study of the diatom spring bloom at Roscoff (France) in 1985. I. The spring bloom within the annual cycle. *Estuar Coast Shelf Science* 25 : 355-367
- Spitz, Y.H., J.R. Moisan, and M.R. Abbott, 2001. Configuring an ecosystem model using data from the Bermuda-Atlantic Time Series (BATS). *Deep Sea Res. II*, 48, 1733-1768.
- Sugimura, Y. and Suzuki, Y., 1988. A high temperature catalytic oxydation method for the determination of non-volatile dissolved organic carbon in sea water by direct injection of a liquide sample. *Mar. Chem.*, 24: 105-131.
- Suzuki, Y. 1993. On the measurement of DOC and DON in seawater. *Mar. Chem.*, 287-288.
- Tréguer, P., Lindner, L., van Bennekom, A.J., Leynaert, A., Panouse, M. and Jacques, G. 1991. Production of biogenic silica in the Weddell-Scotia Sea measured with ³²Si. *Limnol. Oceanogr.*, 36: 1217-1227.
- Veldhuis, M. J. W., and Admiraal, W. 1985. Transfer of photosynthetic products in gelatinous colonies of *Phaeocystis pouchetii* (Haptophyceae) and its effect on the measurement of excretion rate." *Mar. Ecol. Progr. Ser.*, 26, 301-304.
- Veldhuis, M. J. W., and Admiraal, W.1987. Influence of phosphate depletion on the growth and colony formation of *Phaeocystis pouchetii*." *Mar. Biol.*, 95, 47-54.
- Veldhuis, M. J. W., Colijn, F., and Admiraal, W. 1991. Phosphate utilization in *Phaeocystis pouchetii* (Haptophyceae)." *Mar. Ecol.*, 12(1), 53-62.

Watson, S. W., Novitsky, T. J., Quinby, H. L. and Valois, F. W., 1977. Determination of bacterial number and biomass in the marine environment. *Appl. Environ. Microbiol.*, 33: 940-946.

Weisse, T. and Scheffel-Möser, U.1990. Growth and grazing loss in single-celled *Phaeocystis* sp. (Prymnesiophyceae). *Mar. Biol.*, 153-158.



BELGIAN SCIENCE POLICY



WETENSCHAPSSTRAAT 8
RUE DE LA SCIENCE 8
1000 BRUSSELS
www.belspo.be